crystals

MDPI

*Review*

# Manufacturing Techniques for Mg-Based Metal Matrix Composite with Different Reinforcements

**Gurmeet Singh Arora [1,2], Kuldeep Kumar Saxena [1], Kahtan A. Mohammed [3], Chander Prakash [4,5,*] and Saurav Dixit [6,7,*]**

1 Department of Mechanical Engineering, GLA University, Mathura 281406, India; ga211188@gmail.com (G.S.A.); saxena0081@gmail.com (K.K.S.)
2 Pranveer Singh Institute of Technology, Kanpur 209305, India
3 Department of Medical Physics, Hilla University College, Babylon 51002, Iraq; kahtan444@gmail.com
4 School of Mechanical Engineering, Lovely Professional University, Phagwara 144001, India
5 Division of Research and Development, Lovely Professional University, Phagwara 144001, India
6 Peter the Great St. Petersburg Polytechnic University, 195251 St. Petersburg, Russia
7 Division of Research & Innovation, Uttaranchal University, Dehradun 248007, India
* Correspondence: chander.mechengg@gmail.com (C.P.); sauravarambol@gmail.com (S.D.)

**Abstract:** Magnesium is among the lightest structural metals available, with the capacity to replace traditional alloys in mass-saving applications while still providing increased stiffness and strength. The inclusion of reinforcing components into the metallic matrix has a substantial impact on stiffness, specific strength, wear behaviour, damping behaviour, and creep properties when compared to typical engineering materials. Due to their outstanding physical and mechanical characteristics along with low density, magnesium metal matrix composites are viable materials for numerous applications. This study discusses how to choose an appropriate technique and its process parameters for synthesising magnesium-based metal matrix composites (MMCs) and gives an overview of the impacts of various reinforcements in magnesium and its alloys, emphasising their benefits and drawbacks. The essential applications of various magnesium-based MMCs are also critically examined in this article. The impact of reinforcement on the microstructure as well as mechanical characteristics are thoroughly examined.

**Keywords:** magnesium; magnesium composites; carbon nanotubes (CNTs); graphene; graphene nanoplatelets; alumina ($Al_2O_3$); silicon carbide (SiC); boron carbide ($B_4C$)



**Citation:** Arora, G.S.; Saxena, K.K.; Mohammed, K.A.; Prakash, C.; Dixit, S. Manufacturing Techniques for Mg-Based Metal Matrix Composite with Different Reinforcements. *Crystals* **2022**, *12*, 945. https://doi.org/10.3390/cryst12070945

Academic Editors: Huseyin Sevik and Erdem Karakulak

Received: 12 June 2022
Accepted: 27 June 2022
Published: 5 July 2022



## 1. Introduction

Since inception, heavy metals have been used widely for most engineering and industrial applications but they had limitations. Then, alloys were introduced into the market so as to provide a wider range of applications. However, now as the price of crude oil is increasing day by day the parameter of fuel economy is a big reason to worry for most industries. Due to the ability to reduce fuel consumption, lightweight metal matrix composites (MMCs) are attracting quite a lot of attention from modern manufacturers. Low emission of $CO_2$ for environmental protection and reduction in carbon footprint is a major concern for most countries [1–5]. Not only environmental protection but sustainable development is also the need of the hour. Thus, exceptional efforts are being made continuously to bring out the best properties of MMCs [6–13].

Metal matrix composites (MMCs) are becoming more and more popular due to their vast engineering application. The demand for MMCs is most common due to their low cost of manufacturing, ease of fabrication with high productivity. MMCs have been well recognized for superior mechanical properties, better thermal properties and wear resistance in comparison to their unreinforced monolithic counterparts. Various MMCs have been prepared with unique properties for specific applications [14–21]. Al-based,

Mg-based, Ni-based, Ti-based, Cu-based, and Fe-based are a few of them. In such MMCs, Al, Mg, Ni, Ti, Cu and Fe are major matrix materials that cover the maximum percentage of the volume (usually beyond 90%). Whereas, the main role in enhancing the properties and use of MMCs is of reinforcing elements. Reinforcing elements are much less present in MMCs, but influence the properties at a greater level. The reinforcing element could be of different a form such as whiskers, fibres and particulates. The different kinds of usable fibres and particulates are summarised in Table 1.

**Table 1.** Components of MMCs.

| Metal Matrix | Reinforcement | | |
|---|---|---|---|
| | **Whiskers** | **Fibres** | **Particulates** |
| Aluminium (Al)<br>Magnesium (Mg)<br>Nickel (Ni)<br>Titanium (Ti)<br>Copper (Cu)<br>Iron (Fe) | Graphite<br>Cellulose | Jute fibre<br>Kevlar fibre<br>Carbon fibre | SiC<br>$Al_2O_3$<br>Graphene<br>Carbon nanotubes |

Among all biomaterials, Titanium is the most preferred matrix phase of a metal matrix composite [22]. Titanium is a magnificent non-ferrous metal with high specific strength and good corrosion resistance. It is widely used in the chemical, medical, and aerospace industries, where high strength and suitable light weight are critical considerations [23,24]. Titanium and its alloys have also been widely utilised for dental and orthopaedic implants due to their great strength and fracture toughness, as well as their superior biocompatibility [25,26]. Titanium alloy implants frequently fail due to the high friction coefficient of these materials, which can cause the implant to release wear debris into the bloodstream. As a result, inflammation of the surrounding tissue occurs, leading to bone resorption (osteolysis), which eventually causes the implant to loosen, necessitating the replacement of the implant [27,28]. When aluminium is allowed to build up in the body, it can cause bone disease, encephalopathy, and other problems, mostly as a result of renal failure. As long as the amount accumulated in the body is below a threshold level, it does not cause any adverse effects. Composite materials made out of titanium and aluminium have adverse effects on biocompatibility and sustainability. Thus, biocompatible and biodegradable composites are the major concern of implant manufacturers. Magnesium is closer to bone tissue in density, elastic modulus, and yield strength than other metallic implants [29].

Mg MMCs are lightweight, biodegradable and bioactive, provide a better healing rate, suitable degradation in the human body and reduce the chances of a second surgery. The elastic modulus of Mg MMCs also resembles the elastic modulus of the human body enabling it to be more suitable to replace Ti and Al. Additionally, Mg is not reactive as compared to Ti and Al and the body supports the absorption of Mg dissolution [30,31]. However, pure magnesium has a low tensile strength (135 MPa), ductility and hardness. Therefore, reinforcements in Mg are essential to enhance the properties to meet the specific applications. The reinforcement can be metal, ceramic, composite, and polymer but improvement in mechanical properties depends upon the processing technique, types and amount of reinforcement (mechanism of reinforcement) and optimal parameter of reinforcement [32]. The mechanism of reinforcement involves various fabrication techniques, these are powder metallurgy, additive manufacturing, conventional machining, stir casting, liquid infiltration and semi-powder metallurgy. The amount of reinforcement is crucial in regulating the porosity in the composite. The types of reinforcement enable suitable biocompatibility and provide good wettability in the composite [31]. Hence, the mechanism of reinforcement plays a key role in enhancing the mechanical properties of composites.

To overcome the limitations and for obtaining desirable performance, many reinforcing phases have been introduced into the magnesium matrix. By doing so, magnesium metal

composites can have the best application suitable mechanical properties, improved low density, better dimensional stability and damping properties.

The recently used reinforcement with Mg alloy entails the high strength of the Mg MMCs. Graphite-reinforced hybrid composites exhibited a lower wear loss compared to the unreinforced AZ91D alloy and AZ91D–$B_4C$ composites. It was found that with an increase in the $B_4C$ content, the wear resistance increased monotonically with hardness and ultimate tensile strength decreased [32]. AZ31B Mg alloy reinforced by 1.0 vol.% silicon carbide nanoparticles was investigated under quasi-static and impact conditions. The addition of nanoparticles was found to increase the material strength and energy absorption capability though an increase in ductility can be hardly observed [33]. La addition to ZK60 alloy resulted in a formation of a Mg-Zn-La ternary phase, generating a semi-continuous network structure in their as-cast state [34]. The mechanical behaviour of a lanthanum-doped Mg alloy, AZXE7111, (Mg–7Al–1Zn–1Ca–1La, all in wt.%) extruded at different temperatures has been investigated by shen et al. [35]. Malik et al. investigated the higher dynamic mechanical response by adjusting texture through twinning in a ZK61 Mg alloy [36]. Rashad et al. analysed the pure Mg reinforced with 10%Ti and 10%Ti–1%Al particulates were synthesized through the semi-powder metallurgy route followed by hot extrusion [37]. Graphite-reinforced hybrid composites exhibited a lower wear loss compared to the unreinforced AZ91D alloy and AZ91D–$B_4C$ composites analysed by Aattisuhgan [38]. With increasing the concentration of GNPs, the mechanical properties of the composites were gradually improved [39–41].

The major components manufactured using Mg matrix composites are orthopaedic implants, artificial knees, tibial components, bone plates, bone screws, femoral hips, acetabular cups, helicopter transmissions, fan frames of jet engines, control surfaces, structural items, edge flaps, radars, engine blocks, crank cases, transmission cases, etc. [42]. Mg-based metal hydrides can be used as solid-state hydrogen storage materials for fuel cell cars, and as a hydrogen source for fuel cell auxiliary power units [43]. The detailed information about the components manufactured using Mg MMCs in different sectors is showcased in Table 2.

**Table 2.** Applications of magnesium matrix composites.

| Sr. No. | Industry | Applications |
|---|---|---|
| 1 | Aerospace | Helicopter transmission systems<br>Fan frames of jet engines<br>Control surfaces<br>Structural items<br>Edge flaps<br>Spacecrafts<br>Missiles |
| 2 | Automotive | Engine blocks<br>Crankcases<br>Transmission cases<br>Radiator supports<br>Chassis<br>Interiors<br>Door inners |
| 3 | Electronics | Radars<br>Mobile devices<br>Smartphones<br>Computers<br>TVs |

**Table 2.** *Cont.* .

| Sr. No. | Industry | Applications |
|---|---|---|
| 4 | Biomedical | Orthopaedic implants<br>Artificial knees<br>Tibial components<br>Bone plates<br>Bone screws<br>Femoral hips<br>Acetabular cups |
| 5 | Hydrogen storage | Solid-state hydrogen storage |

Even after a wide range of applications, the preparation of magnesium-based composites is very challenging. The prominent challenges that arise in the development of magnesium matrix composites are explained in the next section.

## 2. Challenges in Processing

The challenges that influence the fabrication of magnesium matrix composites are the optimal conditions of processing parameters, complicated fabrication process and secondary deformations in the prepared composites [14,43]. Inert gas (Argon) should be used in the processing to avoid the risk of oxidation. Due care has to be taken to avoid porosities in the composites that decrease the strength of the MMC. The pictorial representation of changes in MMCs preparation is shown in Figure 1.

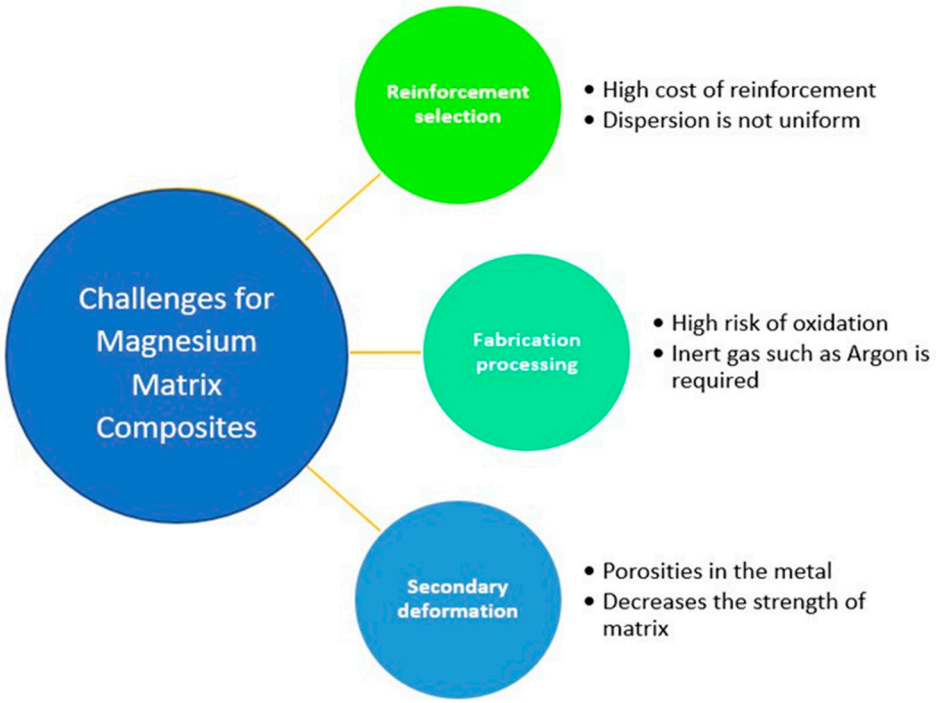


**Figure 1.** Challenges for Mg matrix composites.

Even with so many challenges, the prospects of research in the field of magnesium matrix composites are very lucrative and researchers have been working for the last few decades [1,2]. Moreover, their widely diversified properties develop very strong motivation for further exploration [44,45]. Usually, in MMCs all the challenges are process-based, which could be overcome by selecting the proper processing route/methods, parameters and percentage of reinforcing element. The proven processing routes to develop magnesium-based MMCs are explained in the following section.

## 3. Mg MMCs Development Processes

The processes that are used to develop the metal matrix composites are divided into three broad categories that are solid-state processing, liquid metallurgy processing and powder metallurgy processing. However, magnesium matrix composites are generally produced with a limited number of processes, which lie under these categories and are discussed below.

### *3.1. Solid-State Processing*

MMCs are formed by bonding a metal matrix and a reinforcement phase due to mutual diffusion in solid states at elevated temperatures under the influence of pressure in the solid-state manufacturing process [46]. Most commonly used solid-state processing methods are friction stir processing, diffusion bonding, and additive manufacturing. Friction stir processing is one of the solid-state processes that is majorly used for the fabrication of magnesium-based composites. The complete friction stir process is discussed below.

Friction Stir Processing (FSP)

A pin is pushed into the changed material with the rotating tool's shoulder abutting the base metals during the FSP process. The revolving action of the pin causes metal from each part to flow and form the modified area as the tool (Figure 2) transverses the modified direction under the effect of an applied force. The microstructure that develops during FSP is defined by a central stir zone surrounded by a thermo-mechanically affected zone (TMAZ) and a heat impacted zone and is the outcome of the influence of material flow, plastic deformation, and elevated temperature (HAZ) [45]. Rotational speed, travel speed, tilt angle, tool penetration depth, alloying material, cooling system, and clamping system are the most important parameters in the FSP process. Apart from these factors, tool geometry is also critical. It alters the local microstructure of monolithic specimens to create particular and desirable qualities that are advantageous to the material's performance or requirements [47–53]. The length, diameter, and shape of the pin, as well as the diameter and shape of the shoulder, have a significant impact on the eventual outcome. Some common types of tools used for FSP are straight cylindrical, threaded cylindrical, tapered cylindrical, threaded tapered cylindrical, and square tools [41].

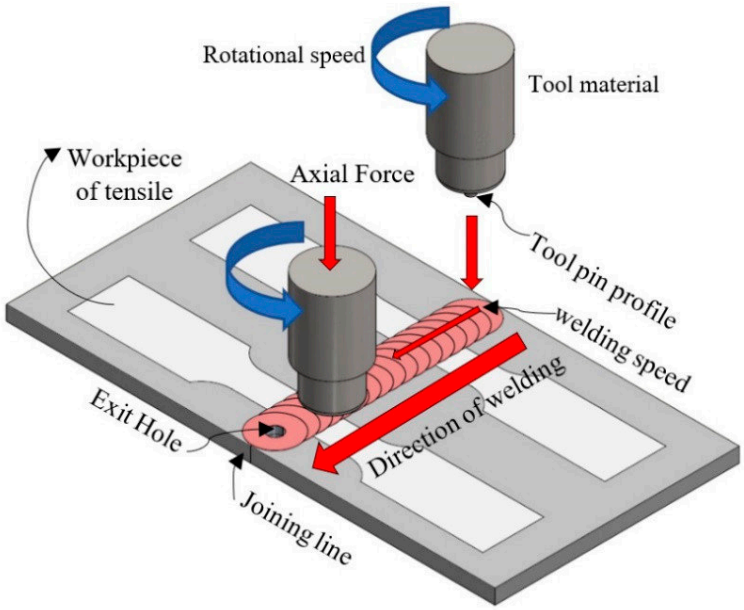


**Figure 2.** A tool and a schematic representation of the friction stir processing procedure [46].

Lu et al. [54] fabricated $Al_2O_3$/CNT-reinforced magnesium matrix (AZ31 alloy) hybrid composite by the Friction Stir processing and evaluated the microhardness and wear

performance. The results showed that the specimen of AZ31 reinforced with 0.2 wt.% $Al_2O_3$ and 0.1 wt.% CNT has shown the highest hardness (112 HV) and the one reinforced with 0.1 wt.% $Al_2O_3$ and 0.2 wt.% CNT has shown lowest wear coefficient.

Whereas, the addition of $Al_2O_3$ reinforced in a magnesium (AZ91 alloy) matrix with 0.8 vol.% $Al_2O_3$ revealed optimum hardness and wear resistance when the rotational speed was 800 rpm and 40 mm/min travel speed [55]. $Al_2O_3$/SiC-reinforced magnesium matrix hybrid composite developed through the FSP technique with 5% SiC and 5% $Al_2O_3$ revealed optimum tensile strength, hardness (69.7 HV) and wear resistance [34]. Titanium-reinforced magnesium (AZ31 alloy) matrix composite having 7, 14 and 21 vol.% Ti particles and AZ31/21 vol.% Ti MMC showed reduced grain size, improved tensile strength and ductility [56]. Nano-hydroxyapatite-reinforced magnesium matrix (AZ31 alloy) composite was fabricated using the Friction Stir processing and observed that the sample made was found to be corrosion resistant and biocompatible for biomedical applications [33].

### *3.2. Liquid-State Processing*

Complex geometries can be created with good interfacial bonding and great dispersion using liquid-state processing, which is cost-effective. Mechanical qualities are improved due to the excellent bonding and homogeneous distribution of reinforcement [35]. The most commonly used liquid metallurgy processes are stir casting, centrifugal casting and squeeze casting. However, stir casting is the most commonly used technique for the development of magnesium matrix composites. The detailed process of stir casting is described below.

#### Stir Casting

Stir casting is a fundamental manufacturing technique for MMCs that takes place in the liquid state. Stir casting promotes the mechanical mixing of reinforcing particles in a molten metal matrix [56–59]. Figure 3 depicts a schematic diagram of the stir casting process. In this process, a crucible is placed inside the resistance heating furnace resting over a sand mould. The thermocouple and a stopper are also attached inside the crucible. The stainless-steel impeller is connected at the end of the mechanical stirrer [60]. In the case of magnesium matrix composites, stir casting is performed in an inert environment. A blanket of argon gas was blown around the melt throughout the composite fabrication process to prevent oxidation reactions. Its advantages are its ease of use, versatility, and capacity to produce huge quantities at a low cost.

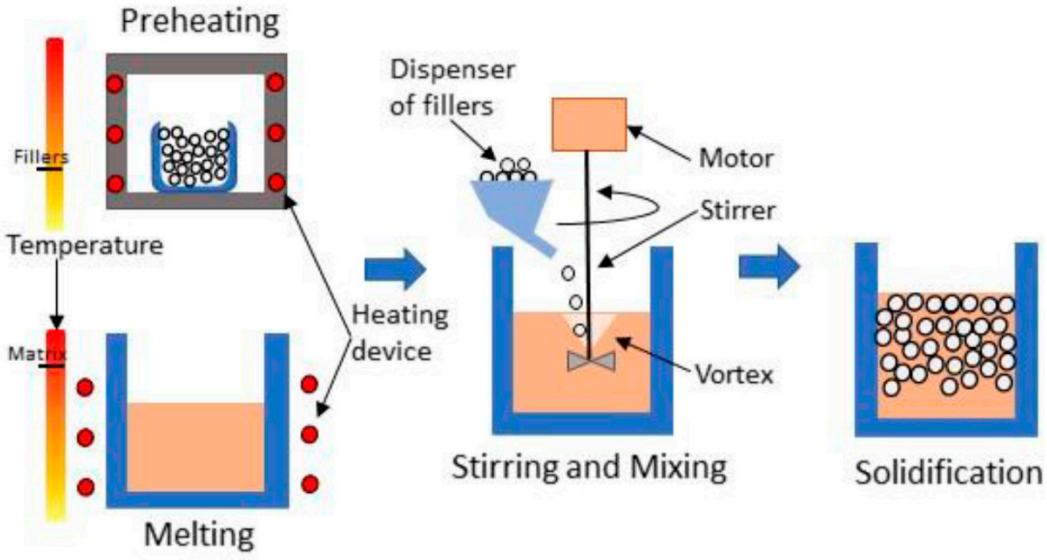


**Figure 3.** Stir casting process [53].

Stir casting is more prominently used in MMCs development and sufficient research work has been carried out on this process [61–68]. In this process, a Mg-based MMC was

prepared using Graphene nanoplatelets at 1.5% and 3%, to find out the effect of varying volume percentage of reinforcement on hardness, tensile and compressive strength. At room temperature, the 3 wt.% GNP specimen showed the highest hardness and UTS while the 1.5% GNP specimen showed the highest UCS [61]. In another study of multiwalled carbon nanotubes reinforced magnesium matrix (AZ31 alloy) composite, fabricated using the stir casting route, 0.1, 0.5 and 1 wt.% of CNTs were added subsequently as reinforcement and it has been noted that hardness increases in proportion to the increase in the percentage of CNTs and ageing further improves it [68]. Density increases while porosity decreases as the percentage of CNTs increases. Stir Casting with ultrasonic treatment was used by Wanga et al. [66] to make a SiC-reinforced magnesium matrix (AZ91D alloy) composite. Composites were prepared with varying percentages of SiC as 5, 10, 15, and 20 wt.% in Mg matrix material. Reported results revealed that the comparatively highest ultimate tensile strength was achieved with 15% SiC when the time used for ultrasonic treatment was 20 min. Similarly, $Al_2O_3$ reinforced magnesium (AZ31 alloy) matrix was prepared by ultrasound-assisted stir casting with 0.5, 1 and 2 wt.% $Al_2O_3$ content. The melt was subjected to ultrasonic treatment in two ways, one outside the furnace (AC-UST) and the other within the furnace (Iso-UST). The hardness increased with an increase in the percentage of $Al_2O_3$ and the values are on the higher side for Iso-UST specimens. The ultimate tensile strength of AC-UST specimens increases as the alumina percentage increases [65].

### *3.3. Powder Metallurgy Processing*

Powder metallurgy (PM) is used to synthesise a wide range of materials. It is a brilliant way to make components with excellent tribological and mechanical properties such as strength, hardness, wear resistance, and impact resistance [69–74].

Figure 4 depicts a schematic diagram of the traditional powder metallurgy routes for the production of metal matrix composites. It begins with the mixing and blending of starting powders, which is accomplished through high-energy ball milling (planetary ball mill) or low-energy ball milling (horizontal shaker), also known as mechanical alloying, and is followed by the consolidation of mixed powders. Consolidation procedures include traditional sintering, hot pressing, spark plasma sintering, and deformation-assisted sintering, among others [36]. Secondary processing of the generated metal matrix composite, such as hot extrusion and hot rolling, is sometimes necessary to attain certain qualities.

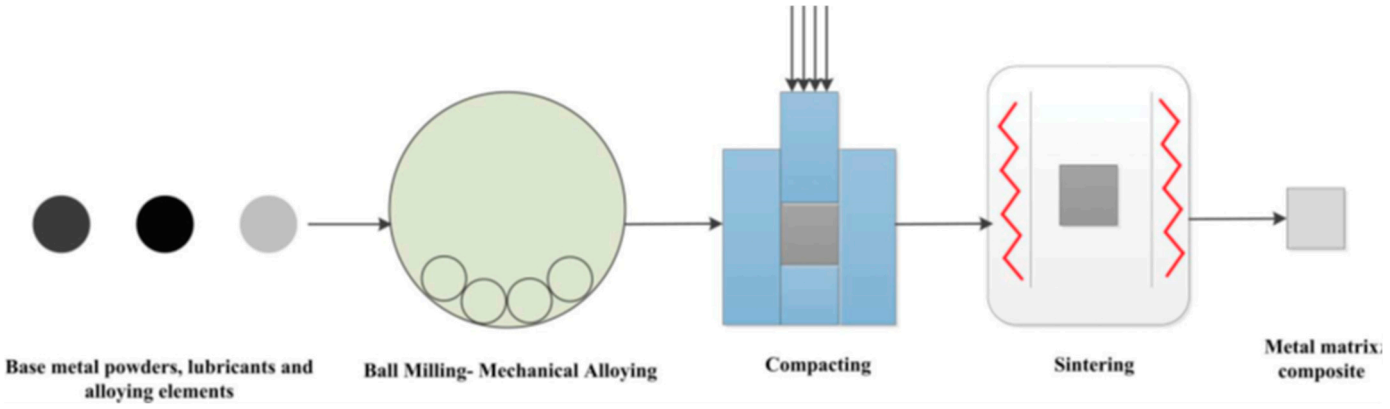


**Figure 4.** Powder metallurgy process.

Bulleted lists look like this: CNT-reinforced Mg powder was prepared by adding 2 wt.% CNTs in the matrix. The Young's modulus of Mg–2 wt.% CNTs improved by 9% when compared to unreinforced Mg and that is validated through resonant measurements. Magnesium matrix and carbon nanotubes were observed to have strong bonding. The rupture strength, strain after fracture and yield strength are all comparable to unreinforced Mg [18]. Nai et al. [14] followed the powder metallurgy route to subsequently fabricate pristine multiwalled carbon nanotubes (0.3%) and Nickel-coated multiwalled carbon-

nanotubes (0.3%)-reinforced magnesium matrix composite. Microhardness and ultimate tensile strength were improved by 41% and 39% in Mg/0.3 wt.% Ni-CNT composite as compared to pure Mg. In a study of multiwalled carbon nanotubes (1%) reinforced magnesium matrix (AZ31 alloy) for the first time, powder metallurgy was used to create composite filler rods for gas tungsten arc welding. When compared to the base metal and unreinforced weld, the CNT-reinforced weld has higher microhardness (67 HV), tensile strength (272 MPa), and yield strength (186 MPa) [19]. When powder metallurgy was employed to make a Nickel-coated carbon-nanotubes-reinforced magnesium matrix (AZ31 alloy) composite, 0.5, 1 and 1.5 wt.% of Ni-CNTs were added subsequently as reinforcement. Yield strength, tensile strength and micro-hardness were improved by 23.48%, 19.35%, and 33.48%, respectively [44].

A detailed comparison among various processes used by researchers for manufacturing Mg composite is shown in Table 3.

**Table 3.** Comparison of various manufacturing processes used for magnesium matrix composite.

| Sr. No. | Components | Process | Key Findings | Reference |
|---|---|---|---|---|
| 1. | AZ91 + 0.8%vol. $Al_2O_3$ | Friction stir processing | Optimum hardness and wear resistance were obtained when the rotational speed was 800 rpm and 40 mm/min travel speed. | [55] |
| 2. | Mg + 5 wt.% SiC and 5 wt.% $Al_2O_3$ | Friction stir processing | Optimum tensile strength, hardness and wear resistance were obtained when rotational speed was 540 rpm and 10 mm/min linear speed. | [41] |
| 3. | AZ31 + 7, 14 and 21 vol.% Titanium particles | Friction stir processing | AZ31/21 vol.% Ti MMC showed reduced grain size, improved tensile strength, and ductility. | [56] |
| 4. | AZ31 + nHA (Nano-hydroxyapatite reinforced) | Friction stir processing | The sample made was found to be corrosion resistant and biocompatible for biomedical applications. | [40] |
| 5. | AZ31 + 18 vol.% Fly ash | Friction stir processing | The grain size is obtained as 6.09 µm and microhardness is obtained as 110.29 VHN. The microstructure had a uniform distribution of Fly ash particles along the stir zone. | [75] |
| 6. | AZ31 + (0.3% CNT, 0.2% CNT + 0.1% $Al_2O_3$, 0.15% CNT + 0.15% $Al_2O_3$, 0.1% CNT + 0.2% $Al_2O_3$, 0.3% $Al_2O_3$) | Friction stir processing | Highest hardness was obtained to be HV112 for AZ31 + 0.2% $Al_2O_3$ + 0.1% CNT specimen. When the load was 1.95 MPa and higher, the wear and friction coefficient of AZ31 + 0.1% $A1_2O_3$ + 0.2% CNTs specimen was lowest among all the specimens. | [54] |
| 7. | AZ91D + 5, 10, 15 and 20 vol.% $Ti_2AlC$ | Stir casting | Yield strength, hardness, compressive strength, and Young's modulus increased with increasing fraction of $Ti_2AlC$, while the optimum UTS was found at 10% $Ti_2AlC$ fraction. | [63] |
| 8. | AZ91 + 12 wt.% TiC | Stir casting | Comparison was made between as-cast and T4 heat-treated specimens. Fracture toughness, microhardness and friction coefficient are higher in the as-cast specimen while wear rate is high in the heat-treated specimen. | [64] |

**Table 3.** *Cont.*

| Sr. No. | Components | Process | Key Findings | Reference |
|---|---|---|---|---|
| 9. | AZ91D + 5, 10, 15, 20 vol.% SiC | Ultrasound-assisted stir casting | Optimum time for ultrasonic treatment was found to be 20 min. Liquid stir for about 5 min improved the distribution of SiC particles. Highest UTS was found at 15% concentration. | [66] |
| 10. | AZ31 + 1.5, 3.0 wt.% Graphene nanoplatelets (GNPs) | Stir casting | At room temperature, the 3% GNP specimen showed the highest hardness and UTS while the 1.5% GNP specimen showed highest UCS. The UTS reduces as the temperature rises from 25 °C to 300 °C. | [54] |
| 11. | AZ31 + 0.1, 0.5, and 1 wt.% CNT | Stir casting | Hardness increases with an increase in % of CNT and ageing further improves it. Density increases while porosity decreases as % of CNT increases. Both mass and volume wear loss decrease with increase in CNT % and the coefficient of friction initially decreases and then remains almost uniform. | [68] |
| 12. | AZ31 + 0.5%, 1% and 2% wt.% $Al_2O_3$ | Ultrasound-assisted stir casting | The melt was subjected to ultrasonic treatment in two ways, one outside the furnace (AC-UST) and the other within the furnace (Iso-UST). The hardness increased with increase in % of $Al_2O_3$ and the values are on the higher side for Iso-UST specimens. The ultimate tensile strength of AC-UST specimens increases as the alumina percentage increases. | [65] |
| 13. | AZ91D + 2, 3, 4 wt.% CNTs | Stir casting | Hardness increases with increase in % of CNT and is highest for 4% CNT specimen on the other hand the specimen having 3% CNT has the highest ultimate tensile strength and yield strength. | [55] |
| 14. | (Mg powder + 2 wt.% CNT) | Powder metallurgy | The Young's modulus of Mg–2 wt.% CNTs improved by 9% when compared to unreinforced Mg and that is validated through resonant measurements. Magnesium matrix and carbon nanotubes were observed to have strong bonding. The rupture strength, strain after fracture and yield strength are all comparable to unreinforced Mg. | [18] |
| 15. | Mg powder + CNT (0.18 wt.%), Al particles (0.5, 1 and 1.5 wt.%) | Powder metallurgy | Optimum hardness and ultimate compressive strength were observed for Mg/1.50 Al + 0.18 CNT specimen. | [15] |

**Table 3.** *Cont.*

| Sr. No. | Components | Process | Key Findings | Reference |
|---|---|---|---|---|
| 16. | (Mg powder + 0.3 wt.% pristine CNT), (Mg powder + 0.3 wt.% Ni-CNT) | Powder metallurgy | The density of the composites did not change significantly, but the porosity did. Microhardness, ultimate tensile strength and ductility were improved significantly in Mg/0.3 wt.% Ni-CNT composite but the same was decreased in Mg/0.3 wt.% CNT composite as compared to pure Mg. | [14] |
| 17. | AZ31 + 1 wt.% CNTs | Powder metallurgy | When compared to the base metal and unreinforced weld, the CNT-reinforced weld had higher microhardness (67 HV), tensile strength (272 MPa) and yield strength (182 MPa). | [19] |
| 18. | AZ31 + Ni-CNT concentrations (0.5, 1, 1.5 wt.%) | Hot-press sintering | Uniform distribution of Ni-coated CNTs was observed. Optimum tensile and microhardness properties were obtained in AZ31/1% Ni-CNT composite. | [44] |
| 19. | Mg powder + CNT contents (2.0, 4.0, 6.0, and 8.0 wt.%) | In situ synthesis followed by powder metallurgy process | The Mg-coated CNTs have shown good interfacial bonding with the Mg matrix. Optimum tensile and microhardness properties were obtained in 4.0 wt.% CNT-Mg composite. | [1] |
| 20. | AZ31 + reduced graphene oxide(r-GO) wt.% (0.2, 0.3, 0.4, 0.5) | Solvent-based powder metallurgy | As the % of r-GO increases the porosity increases and density decreases. At 0.4% r-GO optimum hardness, wear and corrosion properties were obtained. | [76] |

## 4. Process of PM for Mg MMCs

The processing method has a significant impact on the final characteristics of the metal matrix composites. Integration of reinforcement in the magnesium matrix is directly dependent on the process and its parameters. These variables influence the metal matrix composite's final properties and, in turn, its microstructure. A similar concept is also applicable when MMC is prepared through the PM route Figure 5. The development of magnesium metal matrix composites through the PM process and its mechanical properties evaluation has been conducted by many researchers in the last few decades [14–18,21]. Hence, there are multiple reasons to consider the powder metallurgy process as a better technique for processing of MMCs. Among all advantages, one major advantage of the powder metallurgy process is that it provides the possibility to synthesize a large range of compositions [44].

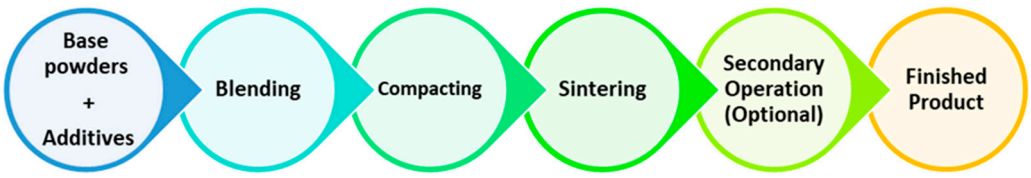


**Figure 5.** Stages of powder metallurgy process.

The detailed steps or methods used in PM are shown in Figure 5. All the stages of the PM process along with the process parameters are discussed in detail in the following sections.

### *4.1. Blending/Mixing*

Traditional powder metallurgy routes for the production of metal matrix composites begin with the blending/mixing of base powders. First, the base powders and additives are mixed to get a homogeneous mixture. Various equipment used for blending such as a Planetary ball mill, V blender, Triaxial ball miller, Horizontal blending machine, Turbula-mixer, etc. Some of the blending devices are shown in Figure 6. During blending/mixing, oxidation is a major concern and therefore, due care has to be taken to avoid oxidation or burning of magnesium by maintaining an inert atmosphere (usually an Argon atmosphere).

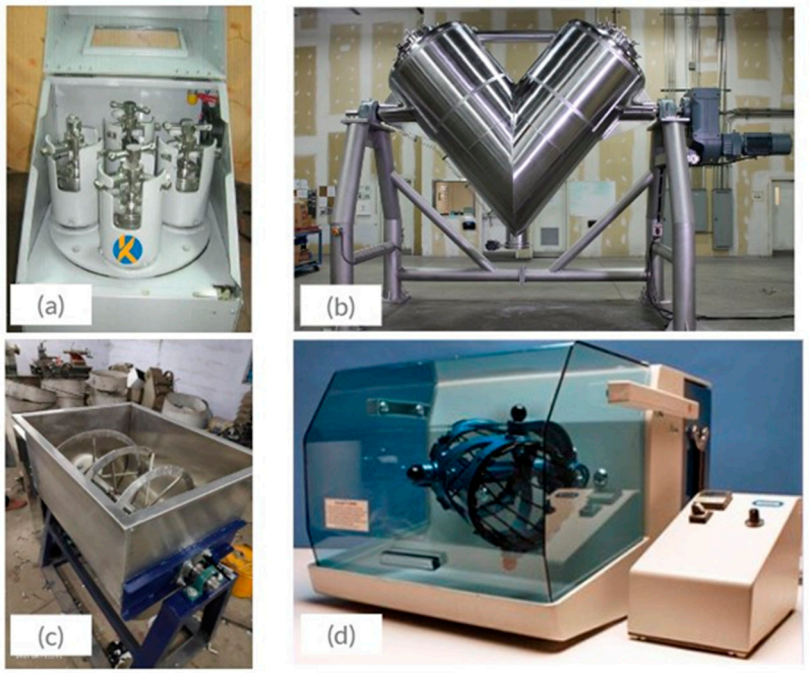


**Figure 6.** Blending devices: (**a**) Planetary ball mill, (**b**) V blender, (**c**) Horizontal blending machine, and (**d**) Turbula-mixer.

The different blending parameters used for different composites are tabulated and shown in Table 4. For the described compositions, the blending speed varies from 40 RPM to 1500 RPM and blending time varies from 1 h to 72 h. When blending time is very high, sufficient breaks of 5 to 10 min are provided in regular intervals.

**Table 4.** Blending parameters for different Mg matrix composites.

| Sr. No. | Matrix Material | Reinforcement | Reinforcement Particle Size | Blending Speed | Blending Time | Reference |
|---|---|---|---|---|---|---|
| 1. | Mg powder | Multiwalled Carbon nanotubes | Diameter = 20 nm | 50 RPM | 10 h | [21] |
| 2. | AZ31 | Multiwalled Carbon nanotubes | Diameter = 50 nm | 300 RPM | 4 h | [19] |
| 3. | AZ91 | Multiwalled Carbon nanotubes | Diameter = 30–50 nm | 800 RPM | 5 h | [76] |
| 4. | Mg powder | Multiwalled Carbon nanotubes | Diameter = 40–70 nm | 200 RPM | 1 h | [15] |
| | | Aluminium powder | 7–15 μm | | | |
| 5. | Mg powder | Multiwalled Carbon nanotubes | Diameter = 40–70 nm | 200 RPM | 1 h | [22] |

**Table 4.** *Cont.*

| Sr. No. | Matrix Material | Reinforcement | Reinforcement Particle Size | Blending Speed | Blending Time | Reference |
|---|---|---|---|---|---|---|
| | | Alumina powder | 50 nm | | | |
| 6. | Mg powder | Ni-coated Carbon nanotubes | Diameter = 10–20 nm | 200 RPM | 1 h | [14] |
| 7. | AZ31 | Ni-coated Carbon nanotubes | Diameter = 10–30 nm | 1500 RPM | 2 h | [44] |
| 8. | Mg powder | Graphene | Thickness = 0.33 nm | 40 RPM | 72 h | [77] |
| 9. | Mg powder | Graphene nanoplatelets | G5: length = 5 µm, thickness = 9 nm<br>G15: length = 15 µm, thickness = 5 nm | 300 RPM | 11 h | [78] |

From Table 4, it is clear that mixing speed is indirectly proportional to the mixing time. In the case of Graphene-reinforced Mg composite mixing speed is kept at 40 RPM while the mixing time was 72 h [21]. In the case of Ni-coated Carbon-nanotubes-reinforced AZ31 composite mixing speed was kept at 1500 RPM and the mixing time was 2 h [78]. Whereas, in the case of GNP reinforcing Mg, to prepare the composite, a mixing speed of 300 RPM for 11 h mixing time was employed [79]. In the case of GNP reinforcement, it is clear that the relation of mixing speed with time is not always indirectly proportional. It has also been observed that in the case of hybrid composites, the mixing speed was kept at 200 RPM and the mixing time was kept at 1 h [15,22]. After successful blending, a compaction process is required.

### *4.2. Compacting*

The second stage of the powder metallurgy process is compacting. In this step, the mixture is compacted under compressive load. Figure 7 shows a schematic depiction of the compaction process. Where the setup is arranged in such a way that, the required amount of mixed powder is admitted inside a die having lower and upper punch. The powder is confined inside by the die wall. A force is applied on the upper punch so as to compress the powder and form the compact.

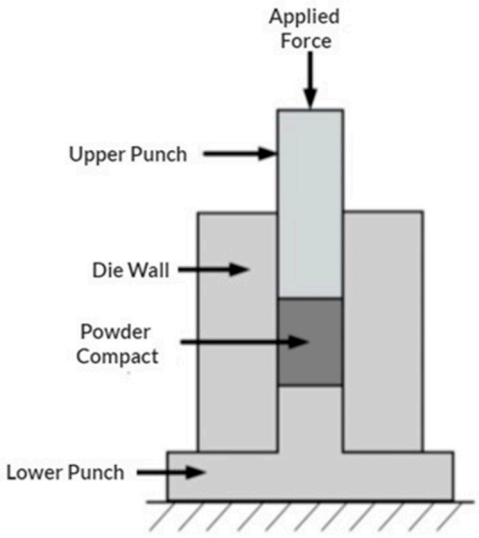


**Figure 7.** Schematic diagram of compaction process.

This process is also known as pressing because of the high pressure applied and the product obtained is known as green compact. Machines such as UTM are for the purpose. For various compositions compacting pressure varies from 25.5 MPa to 728 MPa.

The required shape and size of green compacts are maintained by using a mould or die. The reason for the variation in die dimensions is to get a green compact that is strong enough to endure additional handling operations.

Compacting parameters are summarised in Table 5. From Table 5, it is evident that in the case of multiwalled Carbon-nanotubes-reinforced Mg composite, multiwalled Carbon nanotubes and Aluminium powder reinforced Mg composite, Ni-coated Carbon-nanotubes-reinforced Mg composite and Ni-coated Carbon-nanotubes-reinforced AZ31 composite the height and the diameter of the compact is kept 40 mm and 35 mm, respectively [14,15,21,37]. Whereas, in the case of multiwalled Carbon-nanotubes-reinforced AZ91 composite the height and the diameter of the compact are kept at 120 mm and 6 mm, respectively [77,80].

**Table 5.** Compaction parameters for different Mg matrix composites.

| Sr. No. | Matrix Material | Reinforcement | Compacting Pressure | Compact Size | Reference |
|---|---|---|---|---|---|
| 1. | Mg powder | Multiwalled Carbon nanotubes | 120 MPa | - | [17] |
| | | | 728 MPa | Height = 40 mm, Diameter = 35 mm | [21] |
| 2. | AZ31 | Multiwalled Carbon nanotubes | 500 MPa | Diameter = 20 mm | [19] |
| 3. | AZ91 | Multiwalled Carbon nanotubes | 25.5 MPa | Height = 120 mm, Diameter = 6 mm | [77] |
| 4. | Mg powder | Multiwalled Carbon nanotubes and Aluminium powder | 97 bar (50 tons) | Height = 40 mm, Diameter = 35 mm | [15] |
| 5. | Mg powder | Multiwalled Carbon nanotubes and Alumina powder | 50 tons | Diameter = 35 mm | [22] |
| 6. | Mg powder | Ni-coated Carbon nanotubes | 713 MPa | Height = 40 mm, Diameter = 35 mm | [14] |
| 7. | AZ31 | Ni-coated Carbon nanotubes | 300 MPa | Height = 40 mm, Diameter = 35 mm | [37] |
| 8. | Mg powder | Graphene nanoplatelets | 760 MPa | - | [79] |
| 9. | Mg powder | Silicon carbide particle | 400 MPa | - | [80] |
| 10. | Mg powder | Boron carbide | 50 MPa (Hot pressing at 600 °C) | - | [81] |
| | | | 300 MPa | 25 × 5 × 5 mm | [82] |

### *4.3. Sintering*

Sintering is the third stage of the powder metallurgy process and it usually occurs after compacting. The basic principle of the sintering process is shown in Figure 8. The objective of the sintering process is to use high temperature, pressure, or both to fuse the particles together. Sintering at a high temperature helps to promote stronger particle bonding.

In this stage, all green compacts are now sintered (heated) at a temperature near, but not quite at, the melting point of magnesium (650 °C) in the presence of a layer that acts as an oxidation barrier. For various compositions of Mg, sintering time may vary from 30 min to 6 h. Various methods have been used for sintering such as hot-press sintering, microwave sintering and spark plasma sintering, which are shown in Figure 9 and discussed further in the following sections.

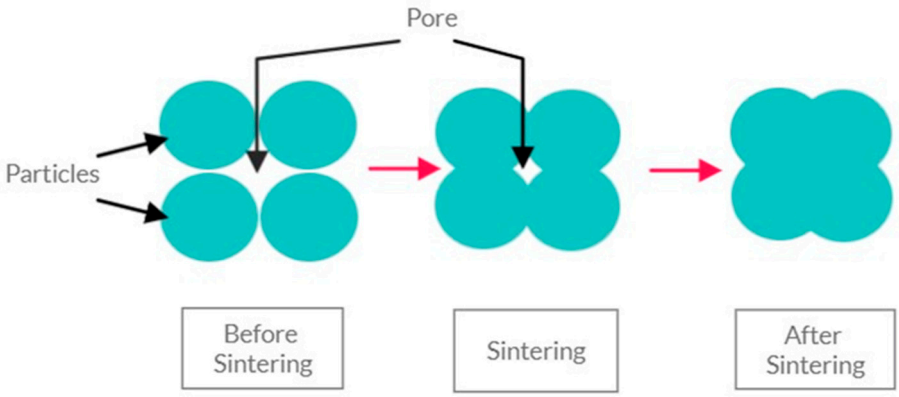


**Figure 8.** Principle of sintering.

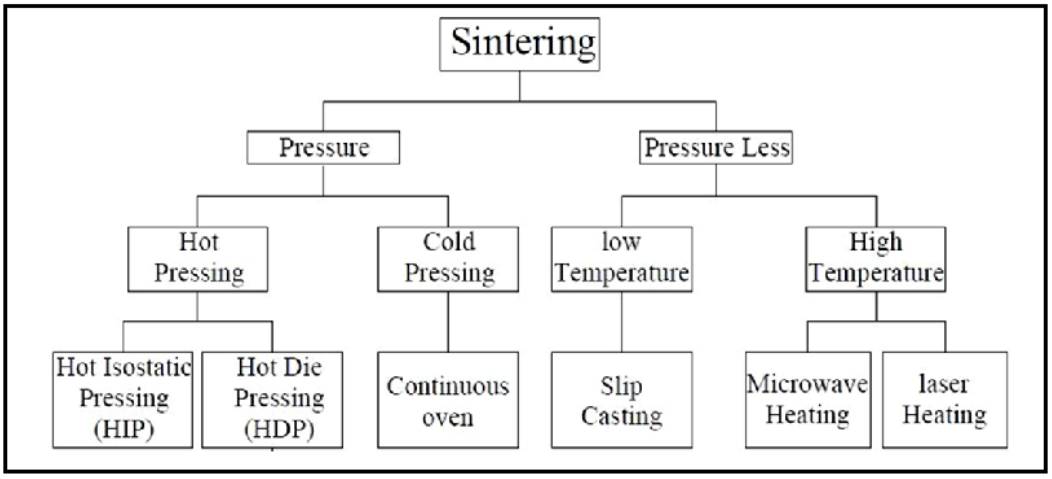


**Figure 9.** Types of sintering process.

#### 4.3.1. Hot-Press Sintering

It is one of the most widely utilised processes because of its controllability and large-scale capabilities. In this process, the sintering is performed under pressure inside a vacuum hot-press sintering furnace. The temperature of the furnace is maintained at around 600 °C.

This process was used to sinter Nickel-coated multi-walled carbon-nanotubes-reinforced AZ31 composite at 15 MPa pressure and 590 °C temperature in 4 h [37]. Whereas, Graphene-reinforced magnesium matrix composites were sintered at a pressure of 25 MPa and temperature of 610 °C in 1.5 h [71]. The process of hot-press sintering is very time-consuming and it involves energy losses as well. Thus, this process is not suitable for applications where time and energy are major constrain.

#### 4.3.2. Microwave Sintering

It is a process in which electromagnetic energy is absorbed volumetrically and converted into heat. Heat is generated inside the material and dissipated throughout the entire volume. The composite materials absorb microwave energy and convert it to heat within their bodies during microwave sintering [55]. This process takes much less time which is why it is also known as microwave rapid sintering.

Through this process, multiwalled Carbon nanotubes and Aluminium powder-reinforced Mg composite was sintered in just 13 min [15]. Whereas, multiwalled Carbon nanotubes and Alumina powder reinforced Mg composite was sintered in 25 min [22]. Due to the rapid processing, this process also saves time and money.

#### 4.3.3. Sparking Plasma Sintering (SPS)

In the case of spark plasma sintering, the mixture is directly put into a graphite mould, and the sintering process is carried out in a vacuum environment using a high pulsed direct current (between 1000 and 3500 A). By causing multiple sparks between particles and establishing a plasma environment, an electrical current can condense the powder in the mould. The composites that were produced have the highest hardness.

Multiwalled Carbon-nanotubes-reinforced Mg composite was sintered through spark plasma sintering under vacuum at 560 °C temperature, 30 MPa pressure and 10 min of holding time [32]. Whereas, Boron carbide reinforced Mg composite was sintered through SPS at 420 °C temperature, 50 MPa pressure under vacuum with 5 min of holding time [83].

The time taken in sintering has a significant impact on increasing the cost of the process and refinement of the microstructure. The time taken in hot-press sintering is in the range of 1.5 to 4 h. Whereas in the case of microwave sintering the time taken is in the range of 13 to 25 min and in SPS the required time is in the range of 5 to 10 min (Table 6). The operation cost of hot-press sintering is high and the setup cost is high in the case of spark plasma sintering. Whereas, microwave sintering has a moderate setup and operation cost. Further, when compared to traditional sintering, microwave sintering requires no holding time. As a result, the duration of time is reduced. Microwave sintering not only improves productivity but also establishes a refined microstructure [22]. The microstructure of the spark plasma sintered sample, on the other hand, reveals a pore-free and uniform distribution of reinforcement particles along the grain boundaries of the Mg matrix.

**Table 6.** Sintering parameters for different Mg matrix composites.

| Sr. No. | Matrix Material | Reinforcement | Sintering Temperature | Sintering Time | Reference |
|---|---|---|---|---|---|
| 1. | Mg powder | Multiwalled Carbon nanotubes | 630 °C | 2 h | [21] |
| 2. | Mg powder | Multiwalled Carbon nanotubes | 560 °C and 30 MPa | 10 min | [32] |
| 3. | AZ31 | Multiwalled Carbon nanotubes | 400 °C | 1 h | [19] |
| 4. | AZ91 | Multiwalled Carbon nanotubes | 550 °C | 5 h | [77] |
| 5. | Mg powder | Multiwalled Carbon nanotubes and Aluminium powder | 640 °C | 13 min | [15] |
| 6. | Mg powder | Multiwalled Carbon nanotubes and Alumina powder | 630 °C | 25 min | [22] |
| 7. | Mg powder | Ni-coated Carbon nanotubes | 640 °C and soaked at 400 °C | 1 h | [14] |
| 8. | AZ31 | Ni-coated Carbon nanotubes | 590 °C and 15 MPa | 4 h | [37] |
| 9. | Mg powder | Graphene | 610 °C and 25 MPa | 1.5 h | [78] |
| 10. | Mg powder | Graphene nanoplatelets | 610 °C | 120 min | [79] |
| 11. | Mg powder | Silicon carbide Particle | 460 °C | 30 min | [80] |
| 12. | Mg powder | Silicon carbide and Alumina powder | 550 °C | 150 min | [83] |
| 13. | Mg powder | Boron carbide | 600 °C | 1.5 h | [81] |
| 14. | Mg powder | Boron carbide | 420 °C and 50 MPa | 5 min | [82] |

### *4.4. Secondary Operation*

It is the fourth and optional stage of the powder metallurgy process. Sometimes in order to enhance some specific properties of the composite obtained through sintering, secondary processing is required to be conducted. Mostly it is conducted for grain refinement, improving the strength and obtaining the required shape of the composite. For metal matrix composites the secondary operations could be hot rolling and hot extrusion. The schematic diagram of the hot rolling and hot extrusion process is shown in Figure 10.

In the case of magnesium metal matrix composite, hot extrusion is performed after sintering as secondary processing. The hot extrusion process uses heated feedstock, called a billet. It is always carried out at temperatures significantly greater than the material's recrystallization temperature. The heated billet is placed in a container, and force is applied to extrude the billet via a die. Table 7 lists the various parameters of hot extrusion. Hot extrusion is used to make parts with precise tolerances and smooth, fine surfaces. Improved microstructures can also be obtained, depending on the metal utilised. The method is also cost-effective because the majority of the metal extruded may be reused.

It is clear from Table 7 that multiwalled Carbon-nanotubes-reinforced AZ31 and AZ91 composite were hot extruded at a temperature of 400 °C and 450 °C, respectively, having extrusion ratios of 5:1 and 9:1, respectively [19,70]. The multiwalled Carbon-nanotubes-reinforced Mg composite, on the other hand, was hot extruded at 350 °C with an extrusion ratio close to 25:1 [14,15,21,22].

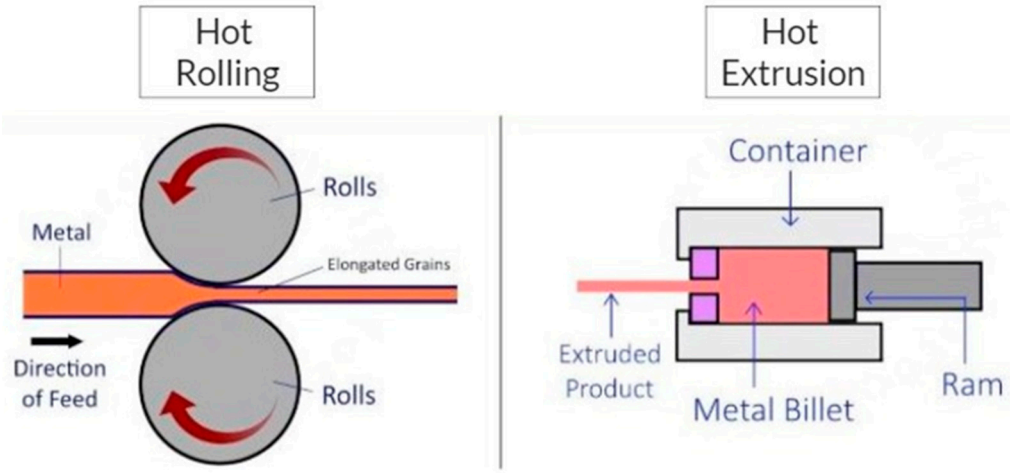


**Figure 10.** Types of secondary processes used in PM.

**Table 7.** Hot extrusion parameters for different Mg matrix composites.

| Sr. No. | Matrix Material | Reinforcement | Extrusion Ratio | Extrusion Temperature | Reference |
|---|---|---|---|---|---|
| 1. | Mg powder | Multiwalled Carbon nanotubes | 25:1 | 350 °C | [21] |
| 2. | Mg powder | Multiwalled Carbon nanotubes and Aluminium powder | 26:1 | 350 °C | [15] |
| 3. | Mg powder | Ni-coated Carbon nanotubes | 25:1 | 350 °C | [14] |
| 4. | AZ31 | Multiwalled Carbon nanotubes | 5:1 | 400 °C | [19] |
| 5. | AZ91 | Multiwalled Carbon nanotubes | 9:1 | 450 °C | [77] |
| 6. | Mg powder | Multiwalled Carbon nanotubes and Alumina powder | 25:1 | 350 °C | [22] |

The powder metallurgy technique is chosen and preferred over the liquid metallurgical route because it is a more direct method of processing that results in a refined microstructure and characteristics for the intended end product. Moreover, the PM route does not consume much energy as is used in the liquid metallurgy route to melt the materials [1,19,44,77].

Powder metallurgy is a realistic and appealing solution since both the matrix material and the reinforcing particles are available in powder form.

## 5. Effect of Reinforcing Elements in Magnesium Matrix Composites

It has been observed that the magnesium matrix composites have been developed using a variety of reinforcing elements successfully to get desired product with suitable properties with respect to the application point of view. Thus, Mg MMCs have depicted exceptional properties as compared to the non-reinforced pure Magnesium [84,85]. The major properties which are most influenced by the reinforcement in Mg are shown in Figure 11.

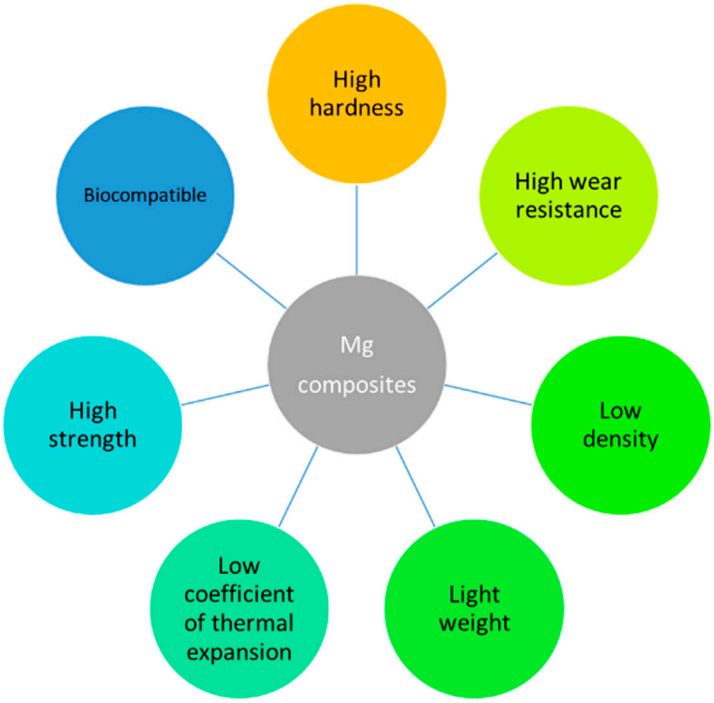


**Figure 11.** Properties of magnesium matrix composite.

Magnesium metal composites are recognised to offer the best mechanical characteristics, enhanced low density, dimensional stability, and damping qualities when the reinforcement phase is chosen properly. Some of the prominent reinforcing elements are Carbon nanotubes (CNTs), Graphene, Graphene nanoplatelets (GNPs), Alumina ($Al_2O_3$), Carbide of Silicon (SiC) and Boron ($B_4C$). The detailed information on reinforcing elements and their effect on the Mg composite are discussed in the following sections.

### *5.1. Carbon Nanotubes (CNTs)*

These are one of the allotropes of carbon in the form of tubes having a diameter dimension of nanometers or less [86]. Usually, CNTs are single wall and multiwall. Multiwalled Carbon nanotubes (CNTs) have been used extensively as reinforcement in the magnesium matrix composite [87–89]. It keeps the density low and improves the overall mechanical properties. Goh et al. [21] used powder metallurgy to manufacture multiwalled carbon-nanotubes-(0.06, 0.18, and 0.3 wt.%)-reinforced magnesium matrix composites. The density of the composites decreased little, but the porosity increased as the CNT content rose. The results of the coefficient of thermal expansion show that Mg–CNT nanocomposites are more thermally stable than monolithic pure Mg. There was no noticeable change in composite hardness and just a minor rise in UTS. The FESEM image in Figure 12 indicates high adhesion between Mg and CNTs, despite the fact that the bonding between Mg and CNTs is believed to be purely mechanical.

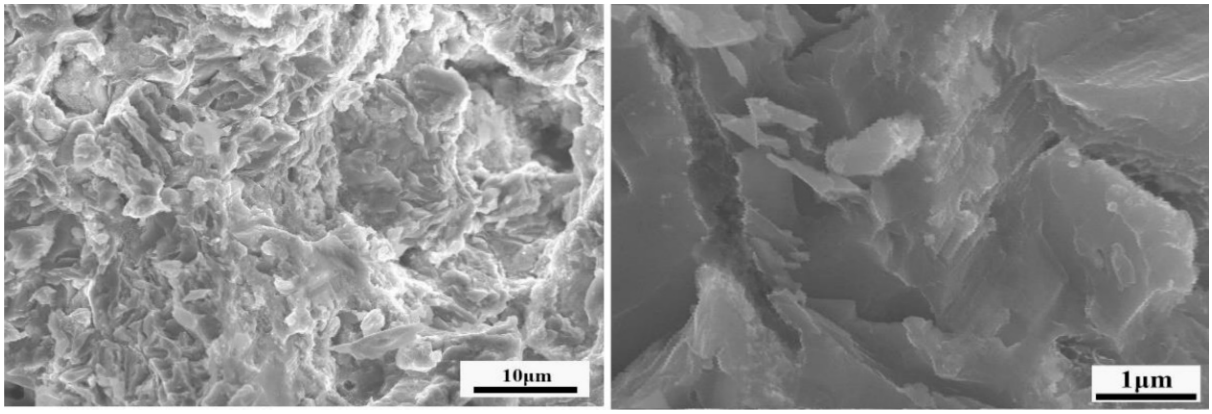


**Figure 12.** FESEM image showing good adherence between Mg and CNT [21].

When CNTs with large aspect ratios are utilised as reinforcement, homogeneous dispersion of CNTs in Mg is a problem, especially at high CNT weight percentages. As the CNTs are so long (up to tens of microns), entanglement between them will eventually result in clustering. Even before tensile testing, these clusters will hinder effective bonding between the Mg particles and CNTs, resulting in minute fissures in the matrix. These fissures invariably operate as nucleation sites for plastic instability, resulting in poorer ductility material failure, clustering of CNTs might result in an increase in porosity in the Mg matrix. The results of the work of fracture (WOF) demonstrate that monolithic pure Mg has a poorer fracture resistance than nanocomposites containing up to 0.18 wt.% CNTs. This is owing to the nanocomposites' increased yield strength and ductility. SEM images of worn surfaces of AZ31-CNTs composites with different weight fraction of CNT is depicted in Figure 13 [22]. The WOF drops as the number of CNTs is increased; this could be due to an increase in clustering effect when the amount of CNTs is increased, which would inevitably lead to porosity.

In a separate investigation, multiwalled short carbon nanotubes reinforced magnesium matrix (AZ91D alloy) composites were used to develop MMCs. As reinforcement, 0.5, 1, 3, and 5 wt.% CNTs were applied. Tensile strength increased initially and then decreased with increase in CNT content. Highest tensile strength was observed for AZ91D/CNT 1% sample. Figure 14 depicts stress–strain curves for pure and nanotube-filled magnesium composites. From Figure 14, it is clear that magnesium alloy containing 1% carbon nanotubes has a tensile strength of 388 MPa, which is comparable to that of commonly used mild steel in automobiles. The uniform distribution of short carbon nanotubes at magnesium grain boundaries could explain why tensile characteristics were considerably improved by adding a small number of carbon nanotubes because, during a triaxial mixing operation, small carbon nanotubes with an average length of 5 nm were thought to impinge relatively uniformly on the near-surface of magnesium alloy powders [70].

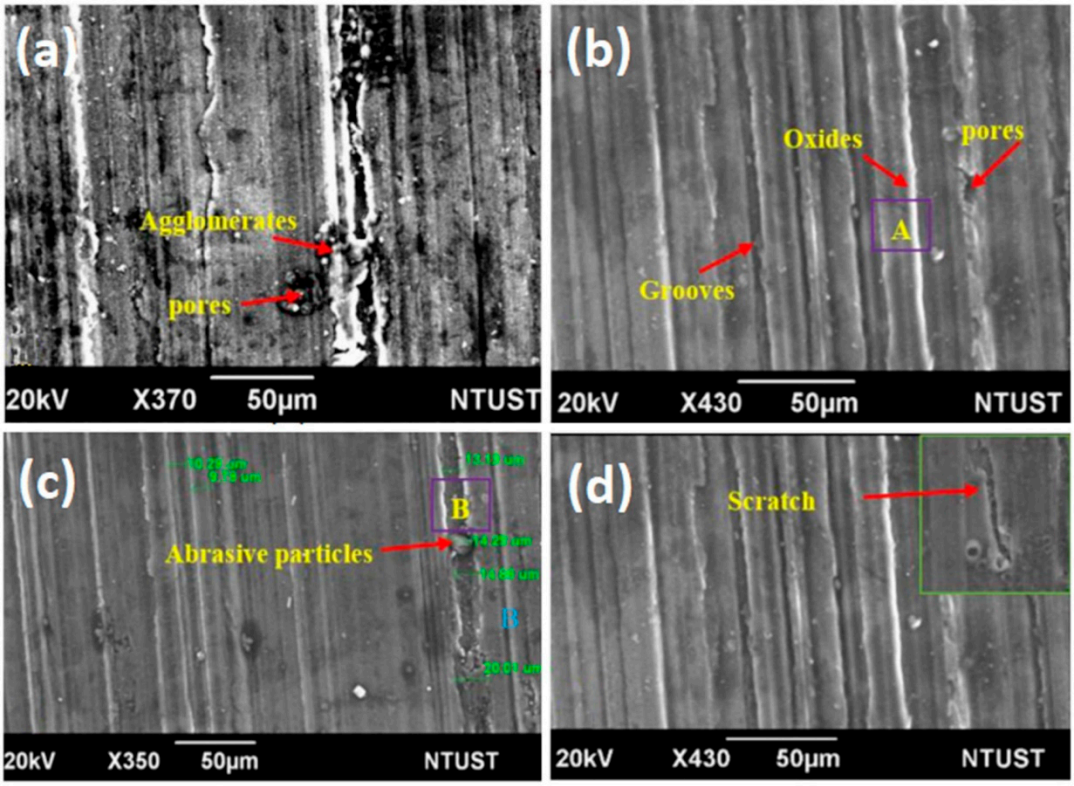


**Figure 13.** Scanning electron microscope (SEM) images of worn surfaces of AZ31-CNTs composites including (**a**) 1.0 wt.%, (**b**) 0.5 wt.%, (**c**) 0.1 wt.%, and (**d**) 0 wt.% of CNTs, under dry sliding conditions [22].

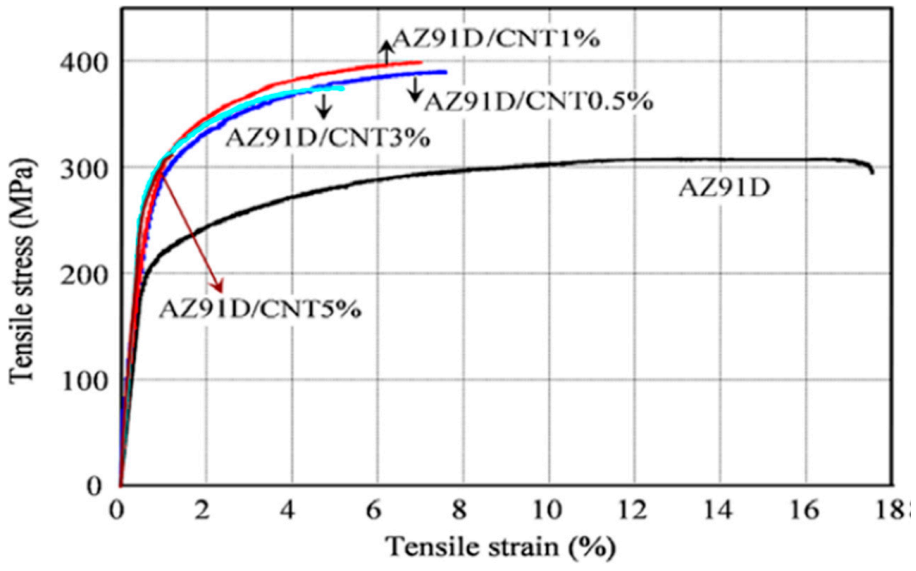


**Figure 14.** Stress–strain curves for AZ91D magnesium alloy composites with and without carbon nanotubes.

The cross-sectional texture of the rods was examined using an electron probe microanalysis (EPMA) to validate the abovementioned interpretation. The majority of carbon nanotubes were found in the area of magnesium grain boundaries, as shown in Figure 15a–c. They were also distributed in a single fibre, as demonstrated in Figure 15d by SEM examination of the etched surface using 0.04 percent hydrochloric acid solutions for 40 s. As a result, when a sufficient amount of carbon nanotubes is introduced, the reinforced

near-surface of the magnesium domains is extremely resistant to deformation, contributing to the increase of tensile characteristics.

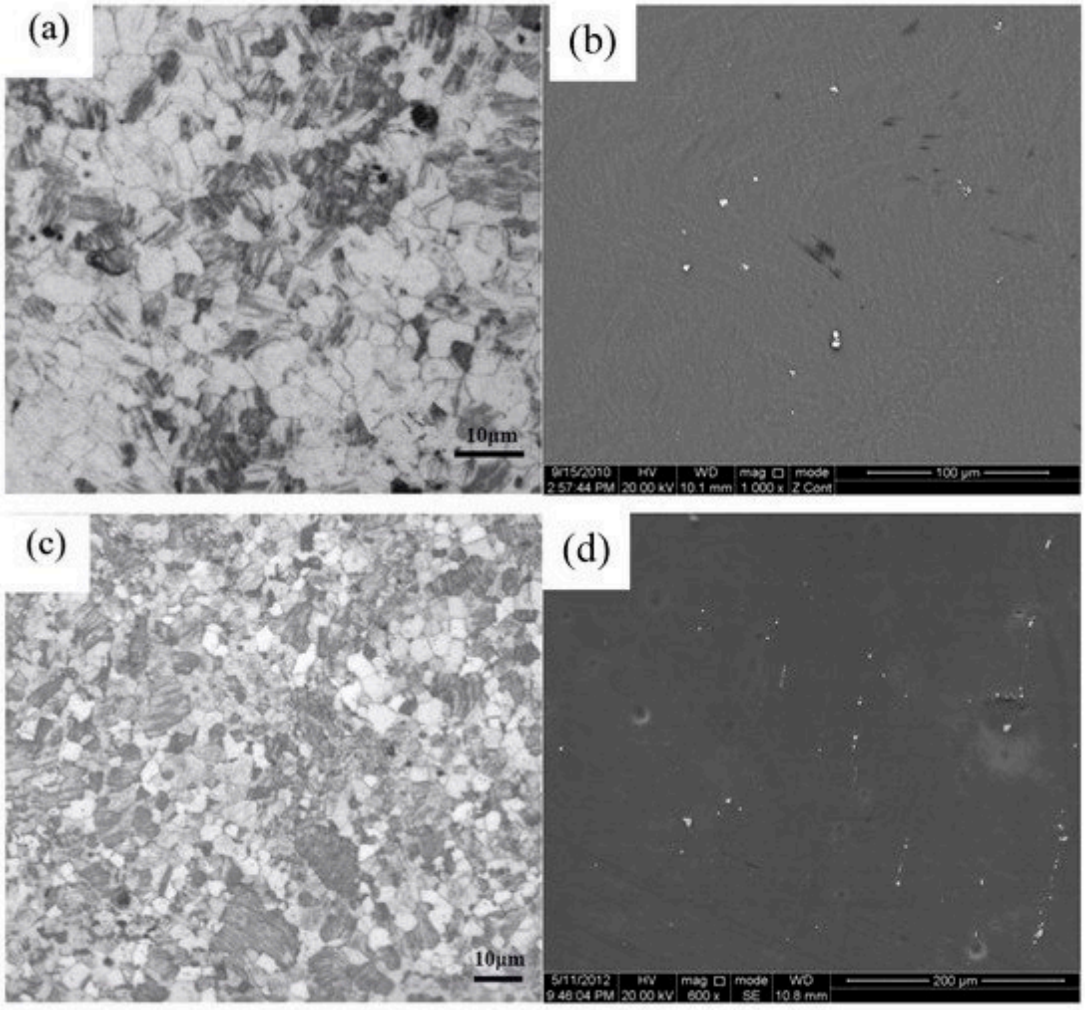


**Figure 15.** Microstructures of the forged alloy and extruded alloy. (**a**,**b**) optical microscope (OM) and SEM image of the forged alloy, (**c**,**d**) OM microstructure of the transverse section and SEM image of the extruded alloy [70].

### *5.2. Graphene*

Graphene is a thin sheet of graphite, that has a thickness on a nanometre scale [90–97]. The use of Graphene as reinforcement enables the magnesium matrix to retain lightweight and increases the overall strength of the composite. Du et al. [71] followed the powder metallurgy route to produce Graphene reinforced magnesium matrix composite. Graphene was added from 0.25 to 1.25 wt.% as reinforcement to create samples. The density of the composites did not vary significantly, but the hardness of the composites rose as the Graphene percentage increased. When compared to pure Mg, the microhardness of the Mg/1.25 wt.% Graphene composite improved by 51%. Figure 16 depicts the effect of graphene weight percent on sample hardness. The effect of two possible important strengthening mechanisms is attributed to the effect of graphene embedded and dispersed inside the Mg grains: (1) the graphene embedded and dispersed inside the Mg grains can block the movement of dislocations within the grains passing through the matrix, making it difficult to reach the grain boundaries at low stress levels; (2) Grain boundary pinning caused by nano-structured graphene dispersed at grain boundary might restrict grain growth in magnesium matrix, resulting in finer magnesium grains. Higher hardness ratings are associated with finer grains.

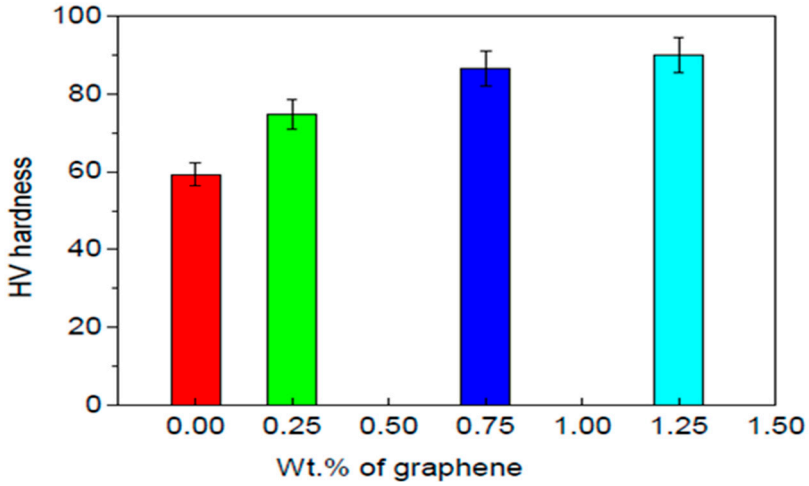


**Figure 16.** The influence of graphene content on microhardness.

Figure 17 shows the SEM analysis of the 1.25 weight percent graphene reinforced Mg matrix composites. The peaks for magnesium, oxygen, and carbon are clearly obtained, as shown in Figure 17b. The presence of graphene in the composites is confirmed by EDS analysis. As a result, these SEM and XRD analyses show that graphene has been successfully incorporated into Mg matrix composites.

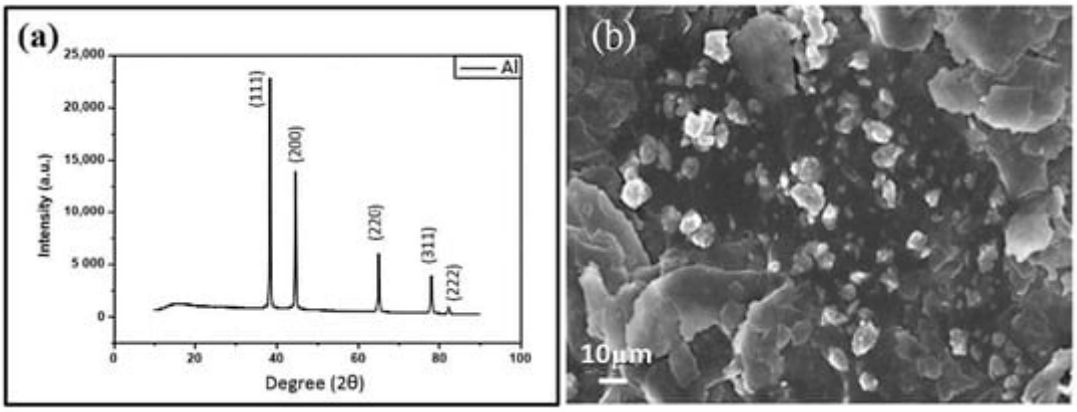


**Figure 17.** Composites' characterization. (**a**) SEM pictures of a composite surface containing 1.25 wt.% graphene; (**b**) XRD image of the composite [71].

*5.3. Graphene Nanoplatelets (GNPs)*

GNPs are also being used as reinforcement for the fabrication of composites that are suitable for biomedical applications [88–91]. Powder metallurgy was used to create a graphene nanoplatelet reinforced magnesium metal matrix composite and 0.1, 0.2, and 0.3 wt.% GNPs were added as reinforcement subsequently. The fabricated composite has come out to be nontoxic and biodegradable. The corrosion resistance and compressive strength increased with an increase in GNPs percentage. Compressive strength was improved significantly in Mg/0.3 wt.% GNP composite [72]. The compressive stress–strain curves of pure Mg and Mg–GNPs composites comprising 0.1–0.3 wt.% G15 and G5 GNPs are shown in Figure 18. When compared to pure Mg, the inclusion of G15 GNPs improved the mechanical characteristics of the Mg matrices significantly. The addition of G15 GNPs, which have fewer layers and fewer flaws in their graphitic structure, enhanced the ductility and compressive strength of the Mg matrices at the same time, as shown in Figure 18a. However, as compared to G15 GNPs, the same G5 GNPs content in Mg resulted in a moderate improvement in mechanical characteristics, as illustrated in Figure 19b.

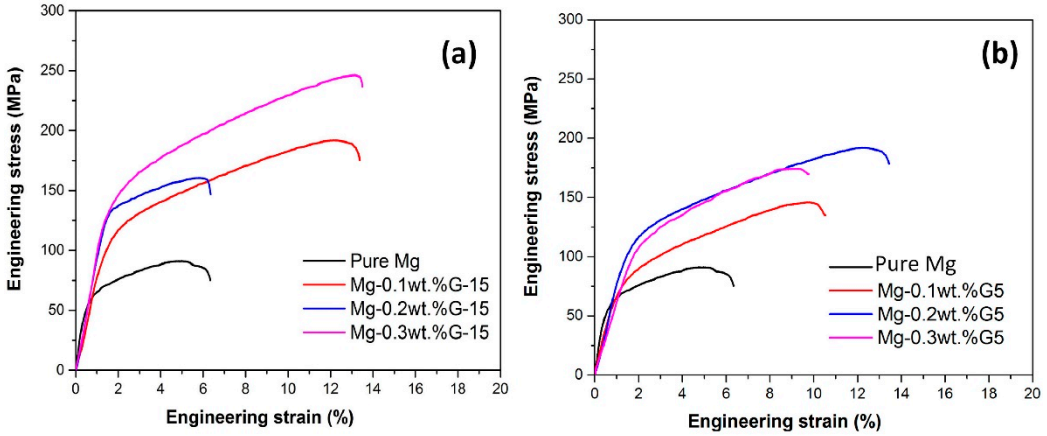


**Figure 18.** Compressive stress–strain curves of pure Mg and its composites containing (**a**) G15 GNPs and (**b**) G5 GNPs [79].

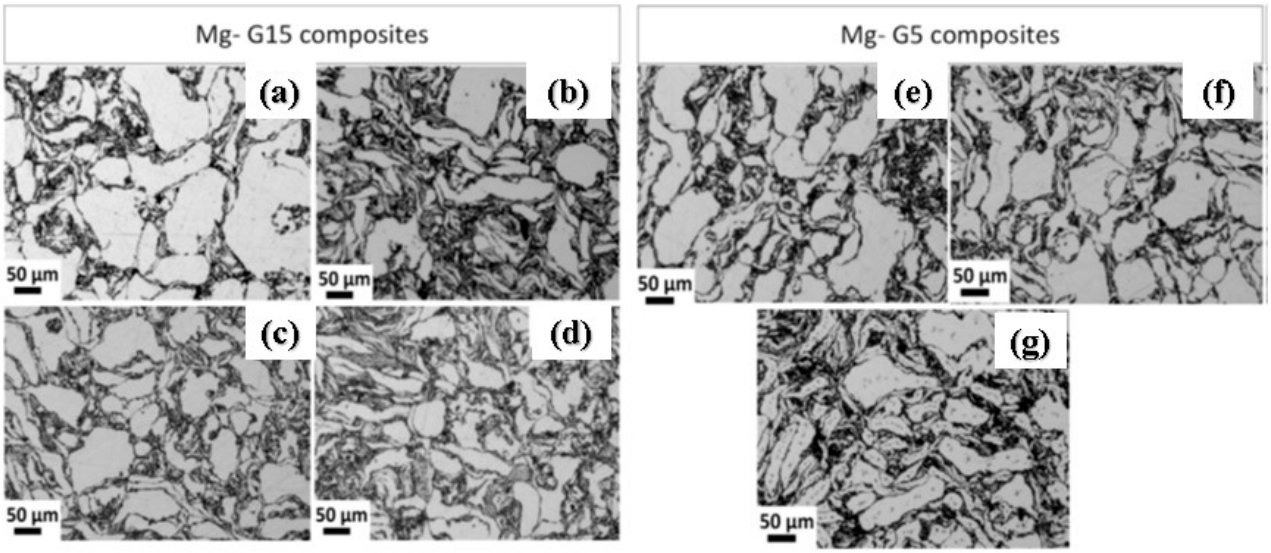


**Figure 19.** Optical microscopy (OM) images of fabricated Mg–GNP composites: (**a**) pure Mg; Mg composites containing (**b**) 0.1 wt.% G15; (**c**) 0.2 wt.% G15; (**d**) 0.3 wt.% G15; (**e**) 0.1 wt.% G5; (**f**) 0.2 wt.% G5; (**g**) 0.3 wt.% G5 [79].

OM images of Mg–GNP composites containing 0.1–0.3 wt.% G15 and G5 GNPs are shown in Figure 20. Microstructural alterations in the Mg metal matrices were caused by the addition of GNPs. Mg (0.1–0.3 wt.%t) G15 composites have smaller granules as compared to pure Mg. Figure 19a–d shows the grain sizes of pure Mg and Mg–GNP composites. The average grain sizes of the Mg matrices shrank as the GNP content increased. The dispersed GNPs were predominantly found near the Mg matrices' grain boundaries, leading to the grain refinement of the matrices. OM of the Mg-G5 composites exhibited higher grain sizes when compared to Mg–GNP composites supplemented with G15 GNPs, as illustrated in Figure 19e–g. The inclusion of GNPs (G5) with a higher number of layers, on the other hand, resulted in agglomeration and an increase in their weight content (0.2–0.3 wt.%) in the Mg matrices.

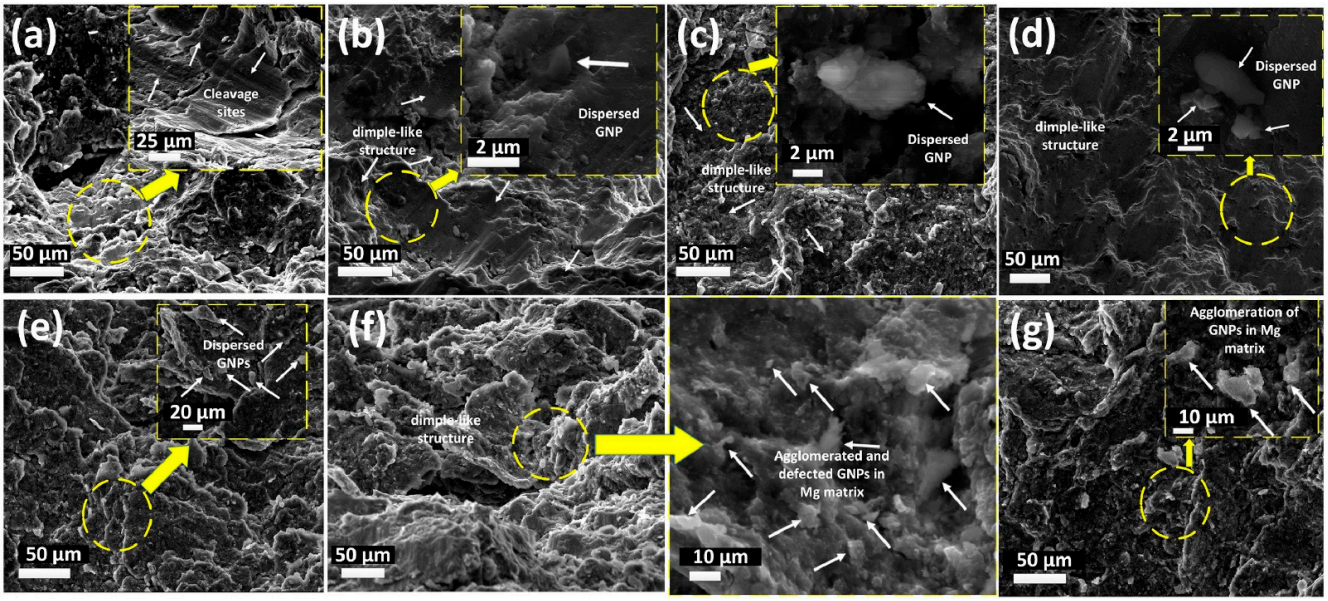


**Figure 20.** After compression testing, SEM photos of the fracture surfaces of pure Mg and Mg–GNP composites: (**a**) pure Mg; (**b**) Mg–GNP composites containing 0.1 wt. percent G15; (**c**) Mg–GNP composites containing 0.2 wt. percent G15; (**d**) Mg–GNP composites containing 0.3 wt. percent G15 GNPs; (**e**) Mg–GNP composites containing 0.1 wt. percent G5; (**f**) Mg–GNP composites containing 0.2, and (**g**) agglomeration of GNP in Mg matrix [79]. The circled area is shown in inset with higher magnification to reveal respective information.

Figure 20 shows the fractured surfaces of pure Mg and Mg–GNP composites comprising 0.1–0.3 wt.% G15 and G5 GNPs. The fracture surface of pure Mg, as shown in Figure 20a, shows the presence of flat surfaces and cleavage characteristics, indicating brittle fractures. The inclusion of GNPs, on the other hand, caused heterogeneous forms of failure in the Mg matrices. Figure 20b–d shows the fracture surfaces of Mg–GNP composites with 0.1, 0.2, and 0.3 wt.% G15 GNPs added, respectively. When compressive stress was applied to Mg matrices containing G15 GNPs, dimple features and uneven lines provided indications of their ductile behaviour. The fracture surface of Mg–0.3 wt.% G15 composites showed uniform dimple structures, suggesting that this batch of composites had predominantly ductile cracks. The fracture surfaces of Mg–GNPs composites containing 0.1–0.3 wt.% G5 GNPs are shown in Figure 10e–g. The fracture surfaces of the Mg–GNPs composites showed cleavage and dimple characteristics, suggesting heterogeneous modes of failure in the Mg matrices reinforced with 0.1 weight percent G5 GNPs, as illustrated in Figure 20e. Agglomerated GNPs, on the other hand, were discovered on the fracture surfaces of composites containing 0.2–0.3 wt. percent G5 GNPs.

### *5.4. Alumina ($Al_2O_3$)*

$Al_2O_3$ is used in hybrid composites of magnesium where more than one reinforcement phase is used [98–100]. Thakur et al. [22] used a powder metallurgy process to fabricate Alumina ($Al_2O_3$) and multiwalled Carbon-nanotube-reinforced magnesium matrix composites. Combinations of Mg-1% CNT, Mg-0.7% CNT + 0.3% $Al_2O_3$, Mg-0.5% CNT + 0.5% $Al_2O_3$, Mg-0.3% CNT + 0.7% $Al_2O_3$ were made subsequently. Macrohardness, microhardness and tensile strength were increased as the $Al_2O_3$ content increased in the reinforcement. Optimum values of macrohardness, microhardness and tensile strength were observed for Mg-0.3%CNT + 0.7% $Al_2O_3$ sample. The failure was found to be fundamentally brittle after fracture analysis of the composites. The existence of cleavage-like characteristics was discovered when the fracture surfaces were examined at high magnification. The matrix contained several macroscopic and tiny microscopic fractures. SEM studies confirmed the presence of several deep macroscopic cracks in the Mg-1 wt.% CNT composite. The inferior

mechanical strength of Mg-1 wt.% CNT during tensile loading could be explained by its enhanced brittleness [101–113].

Whereas, in Alumina ($Al_2O_3$) and SiC reinforced magnesium matrix hybrid composite, combinations of Mg-5% SiC + 5% $Al_2O_3$, Mg-10% SiC + 10% $Al_2O_3$, Mg-15% SiC + 15% $Al_2O_3$ were made subsequently through the powder metallurgy route. Density was raised when reinforcement content was increased. The hardness of reinforced Mg was higher than the non-reinforced Mg and the highest hardness was observed for Mg-10% SiC + 10 wt.% $Al_2O_3$ sample and the sample of Mg-5% SiC + 5 wt.% $Al_2O_3$ displayed the highest wear resistance. Figure 21 depicts the graph plotting Vicker's hardness number on the percentage of specimen reinforcements. The graph shows that the hardness of magnesium metal matrix composites increases as the weight proportion of alumina and silicon carbide (up to 10%) increases relative to the base metal. The addition of 5% and 10 wt.% SiC and $Al_2O_3$ to pure magnesium increased the hardness of the material, as seen in the graph. It is possible that the tougher silicon carbide and alumina particles are to contribute. The presence of these particles increases the hardness of composites by providing additional resistance to plastic deformation. However, the hardness of SiC and $Al_2O_3$ reinforced composites with a 15 wt.% SiC and $Al_2O_3$ content was reduced due to insufficient interface bonding between matrix and reinforcement particles [83].

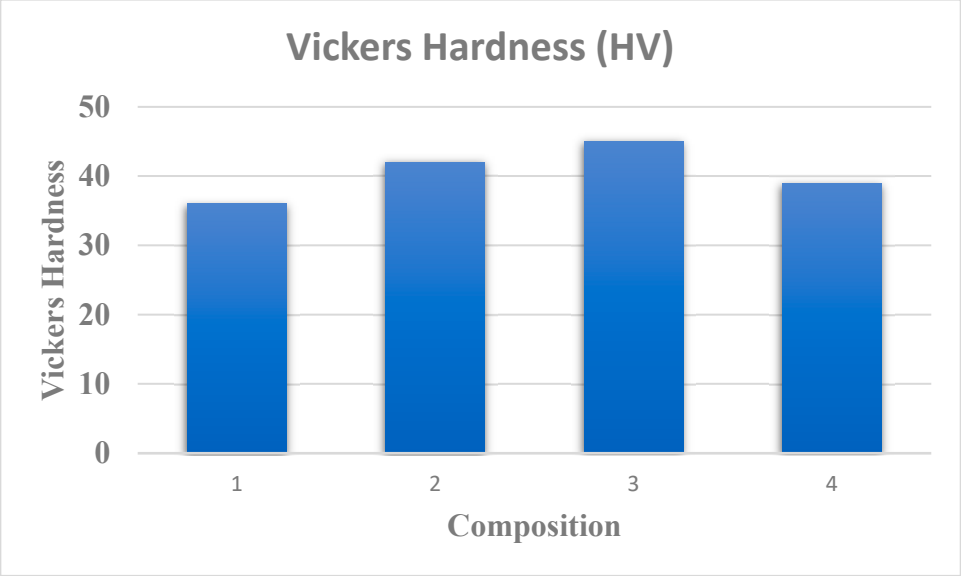


**Figure 21.** Vickers hardness number for pure Mg, Mg-5% SiC + 5% $Al_2O_3$, Mg-10% SiC + 10% $Al_2O_3$ and Mg-15% SiC + 15% $Al_2O_3$.

For Mg matrix material with 0%, 5%, and 10 wt.% SiC and $Al_2O_3$ reinforcement, the microstructure of sintered specimens has been investigated. The presence of SiC and $Al_2O_3$ reinforcements in the magnesium matrix composites can be seen in the SEM micrograph. The samples had a homogenous particle distribution, and pore flaws were generated in select sections of the microstructure. As indicated in Figure 22, greater bonding between reinforced particles and matrix was achieved.

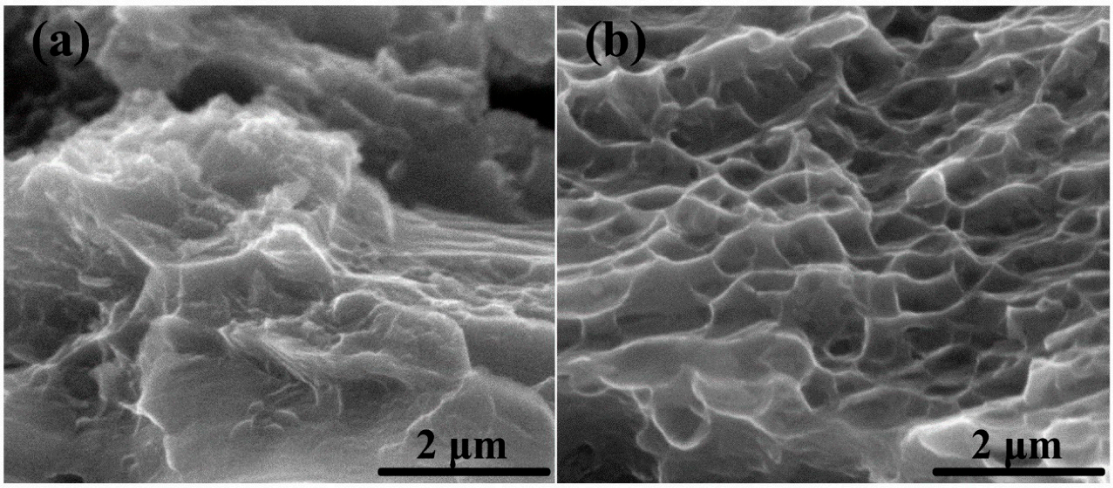


**Figure 22.** Mg composites strengthened with SiC and $Al_2O_3$, optical micrographs (**a**) 5%, and (**b**) 10% [76].

*5.5. Silicon Carbide (SiC)*

The use of Silicon carbide (SiC) as reinforcement in metal matrix composites has evolved over the years significantly. Different particle sizes of SiC are used to reinforce magnesium matrix composite [114,115]. Following that, 10%, 20%, and 30 wt.% SiC particles were added as reinforcement in Mg MMCs. Although the density of the composites did not change significantly, the porosity did. Hardness, tensile strength and compressive strength were improved significantly in Mg/30 wt.% SiC particulate composite in Figure 23 [80].

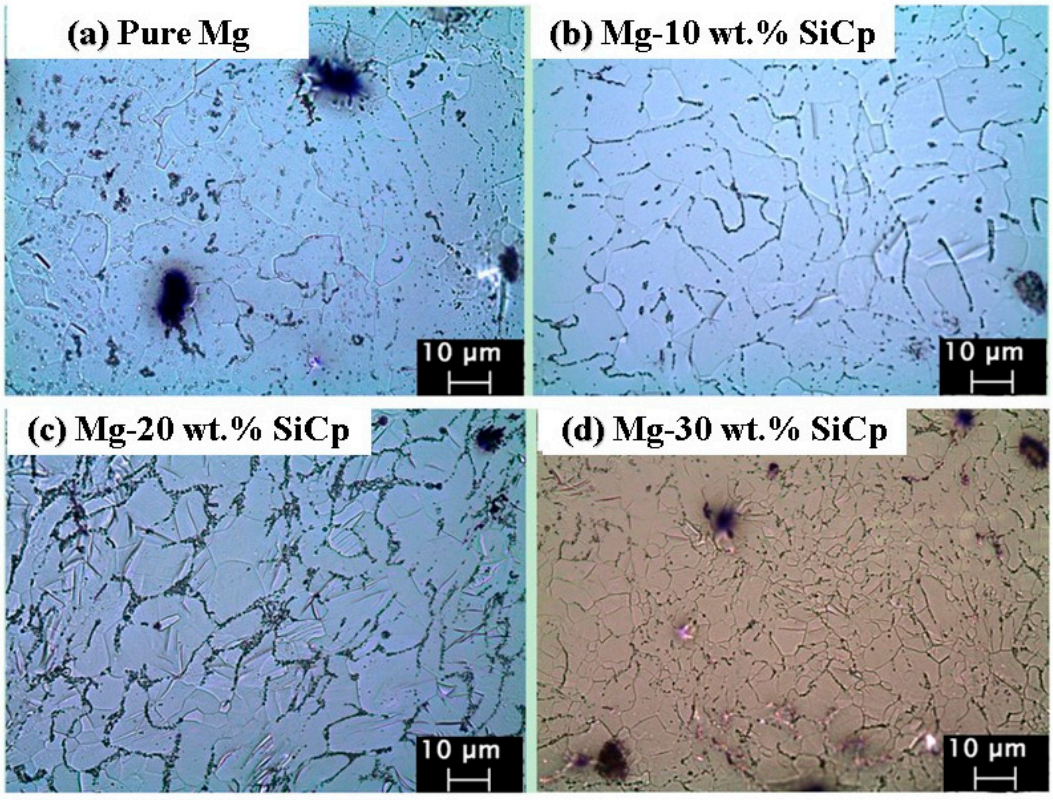


**Figure 23.** Micrographs (**a**) Pure Mg (**b**) Mg-10 wt.% SiCp; (**c**) Mg-20 wt.% SiCp; and (**d**) Mg-30 wt.% SiCp composites [80].

Scanning electron microscopy was used to analyze the microstructures of powder metal Mg-SiCp composites containing 10 to 30 percent SiCp. SEM micrographs of Mg-SiCp composites containing 10, 20, and 30% SiC particles are shown in Figure 14. The SiC particles are evenly dispersed in the magnesium matrix, as evidenced by the micrographs. The micrograph showed SiC particles. After sintering, the bonding between magnesium and SiC particles is more strong.

### *5.6. Boron Carbide ($B_4C$)*

$B_4C$ has low density, hardness, abrasion resistance and high thermal stability [104–106]. It has been used widely as a reinforcement phase in magnesium matrix composites. In a study of $B_4C$ reinforced magnesium matrix composite, 10, 20 and 30 wt.% $B_4C$ was added subsequently as reinforcement and the powder metallurgy process was applied. The density of the composite did not vary significantly, but its porosity did. The hardness of reinforced Mg was higher than the non-reinforced Mg and the highest hardness was observed for Mg + 30% $B_4C$ sample. UCS decreased in reinforced composites as compared to pure Mg. The wear resistance increased with an increase in reinforcement content [74]. SEM pictures of pure Mg and MMCs are shown in Figure 24. In pure Mg, grain boundaries can be seen clearly. All composites have a homogeneous dispersion of particles, as evidenced in SEM pictures of MMCs. In Mg-10 wt. percent $B_4C$ and Mg-20 wt. percent $B_4C$, no agglomeration of $B_4C$ particles was detected. However, partial agglomeration may be seen in Mg-30 wt. percent $B_4C$. Due to the low porosity content, micro and macro porosities do not show up in the microstructure. Pure Mg has an average particle size of 124 µm, while grain sizes of 10, 20, and 30 wt. percent $B_4C$ composites are 99, 84, and 92 µm, respectively. As a result, $B_4C$ particles found near grain borders can be considered to restrict grain coarsening.

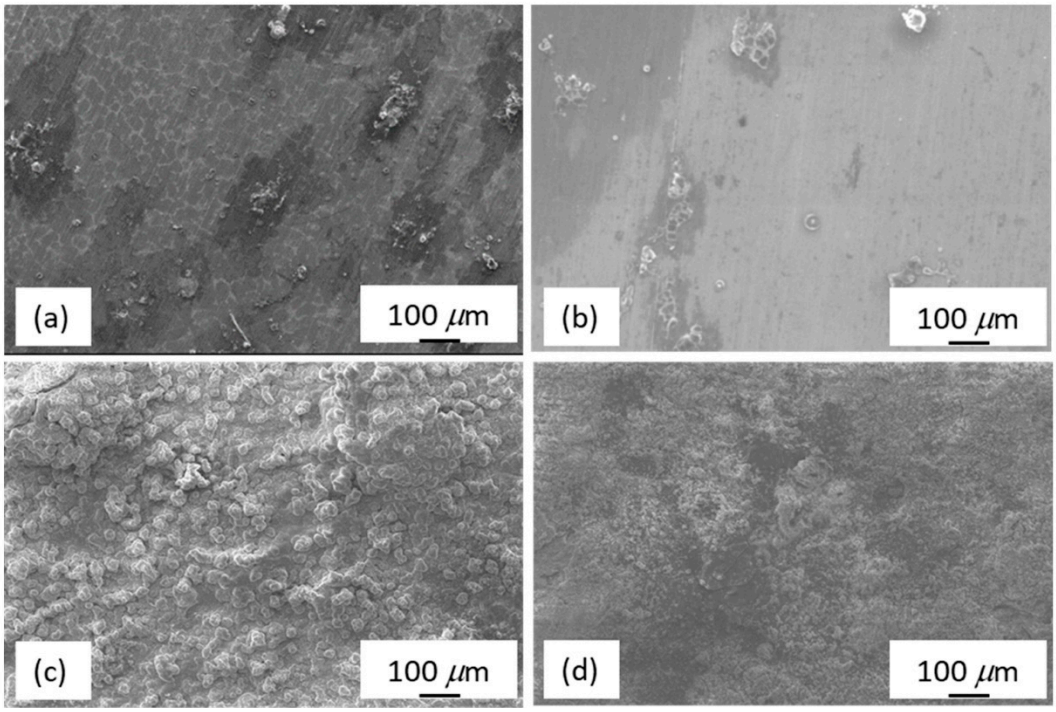


**Figure 24.** SEM of (**a**) pure Mg, (**b**) Mg-10 wt.% $B_4C$, (**c**) Mg-20 wt.% $B_4C$, (**d**) Mg-30 wt.% $B_4C$ [81].

Ghasali et al. [82] followed powder metallurgy using spark plasma and microwave sintering, respectively, to fabricate $B_4C$ (10 wt.%) reinforced magnesium metal matrix composite. Density was decreased when the microwave sintering process was used. However, bending strength and hardness were improved when spark plasma sintering was used. The microstructure of SPS and microwave sintered samples in Figure 25 shows a uniform dispersion of $B_4C$ particles. However, certain gaps in the microstructure of microwave

sintered sample with a diameter of 200 µm have formed as a result of pulling out magnesium particles during grinding due to inadequate Mg-Mg bonding in the sample sintered in the microwave. Another probable explanation is that due to the huge particle size of magnesium turnings, there is a considerable percentage of porosity in the pressed sample (almost 30%). The microstructure of the SPS sintered sample, on the other hand, reveals a pore-free and uniform distribution of $B_4C$ particles along the grain boundaries of the Mg matrix.

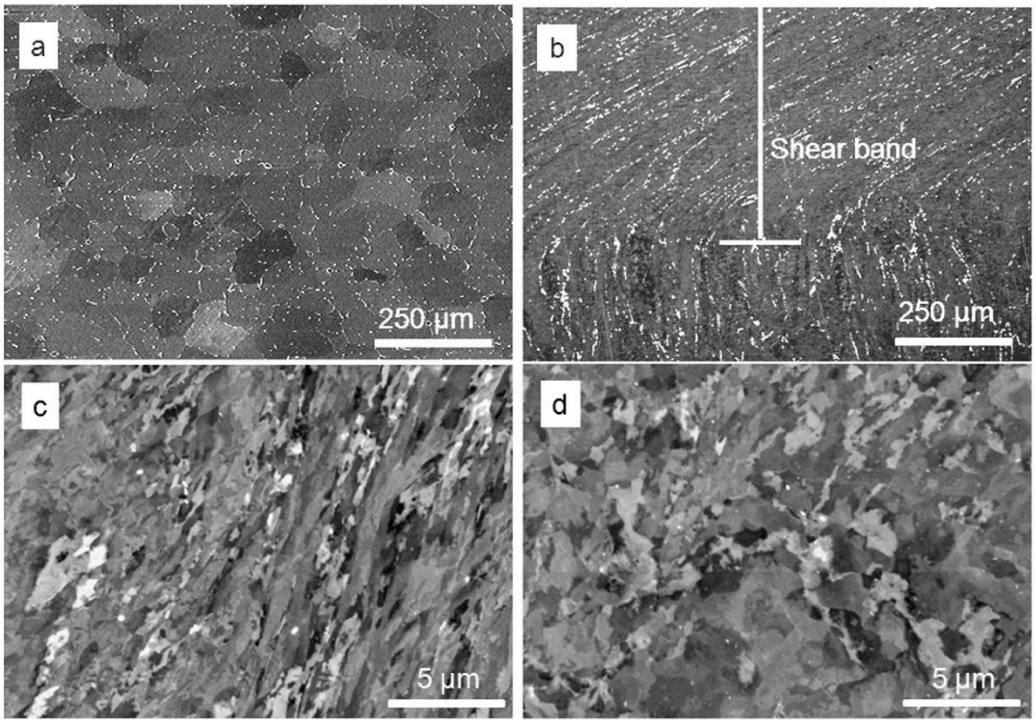


**Figure 25.** Microwave (**a**,**b**) and spark plasma (**c**,**d**) sintered samples backscattered micrographs [82].

The mechanical properties obtained by using various reinforcement phases in the Mg matrix are showcased in Table 8.

**Table 8.** Mechanical properties of different Mg matrix composites.

| Sr. No. | Components | Ratio | Mechanical Properties | | | | Reference |
|---|---|---|---|---|---|---|---|
| | | | Hardness | Tensile Strength | Compressive Strength | Bending Strength | |
| 1. | Mg powder, Graphene | Graphene wt.% (0.25–1.25) | 89.9 HV | - | - | - | [78] |
| 2. | AZ31, reduced graphene oxide | Reduced graphene oxide wt.% (0.2, 0.3, 0.4, 0.5) | 64.6 HV | - | - | - | [76] |
| 3. | Mg powder, Graphene nanoplatelets (GNPs) | GNPs 0.1, 0.2, and 0.3 wt.% | - | - | 246 MPa | - | [79] |
| 4. | Mg powder, Graphene nanoplatelets (GNPs) | GNPs 0.3 wt.% | 68.5 HV | 238 MPa | - | - | [107] |

**Table 8.** *Cont.*

| Sr. No. | Components | Ratio | Mechanical Properties | | | | Reference |
|---|---|---|---|---|---|---|---|
| | | | Hardness | Tensile Strength | Compressive Strength | Bending Strength | |
| 5. | Magnesium powder, Aluminium powder Graphene nanoplatelets (GNPs) | Mg-0.5 Al + 0.18 GNPs Mg-1.0 Al + 0.18 GNPs Mg-1.5 Al + 0.18 GNPs | 60 HV | 268 MPa | - | - | [108] |
| 6. | Magnesium powder, Copper powder Graphene nanoplatelets (GNPs) | Mg-1 Cu + 0.18 GNPs Mg-1 Cu + 0.36 GNPs Mg-1 Cu + 0.54 GNPs | 56.7 HV | 260 MPa | 420 MPa | - | [6] |
| 7. | Mg powder, SiC particulate | SiCp 10, 20 and 30 wt.% | 90 HRB | 87.38 MPa | 122.71 MPa | | [80] |
| 8. | Mg powder, SiC, $Al_2O_3$ | Mg-5% SiC + 5% $Al_2O_3$, Mg-10% SiC + 10%$Al_2O_3$, Mg-15% SiC + 15% $Al_2O_3$ | 45.39 HV | - | - | - | [83] |
| 9. | Mg powder, $B_4C$ | 10, 20 and 30 wt.% $B_4C$ | 70 HV | - | 204.73 MPa | - | [81] |
| 10. | Mg powder, $B_4C$ | 10 wt.% $B_4C$ | 92 HV | - | - | 191 MPa | [82] |
| 11. | Magnesium powder of 98.5% pure, Alumina ($Al_2O_3$) 50 nm size, multiwalled carbon nanotube | Mg-1%CNT, Mg-0.7% CNT + 0.3%$Al_2O_3$, Mg-0.5% CNT + 0.5% $Al_2O_3$, Mg-0.3% CNT + 0.7% $Al_2O_3$ | 44.2 HV | 196 MPa | - | - | [22] |
| 12. | Multiwalled CNT and Magnesium powder 98.5% pure | CNT concentrations 0.06, 0.18 and 0.3 wt.% | 44 HR15T | 210 MPa | - | - | [21] |
| 13. | AZ91D, Multiwalled short CNTs | CNT contents (0.5, 1.0, 3.0, and 5.0 wt.%) | - | 388 MPa | - | - | [77] |
| 14. | Multiwalled CNT and Magnesium powder 99.8% pure | Mg + 2 wt.% CNT | - | 140 MPa | - | - | [18] |
| 15. | Multiwalled CNT, Magnesium powder 99.9% pure and carbamide 99% pure | CNT concentrations (0.05 and 1 wt.%) and overall porosities (20, 30, and 40 %) | - | - | 87.5 MPa | - | [17] |

**Table 8.** *Cont.*

| Sr. No. | Components | Ratio | Mechanical Properties | | | | Reference |
|---|---|---|---|---|---|---|---|
| | | | Hardness | Tensile Strength | Compressive Strength | Bending Strength | |
| 16. | Magnesium powder 98.5% pure, Carbon nanotubes, Aluminium powder | Mg-0.18% CNT + 0.5% Al, Mg-0.18% CNT + 1.0% Al, Mg-0.18% CNT + 1.5% Al | 60 HV | - | 421 MPa | - | [15] |
| 17. | Magnesium powder 98.5% pure, pristine multiwalled carbon nanotubes, Nickel-coated multiwalled carbon nanotubes | Mg + 0.3 wt.% pristine CNT, Mg + 0.3 wt.% Ni-CNT | 55 HV | 237 MPa | - | - | [14] |
| 18. | AZ31, Multiwalled CNTs | 1 wt.% CNTs | 67 HV | 272 MPa | - | - | [19] |
| 19. | AZ31, Nickel-coated multiwalled carbonnanotubes | CNT contents (0.5, 1.0 and 1.5 wt.%) | 61.88 HV | 296 MPa | - | - | [44] |
| 20. | Magnesium powder 99.5% pure, Carbon nanotubes | Mg + 2% CNT, Mg + 4% CNT, Mg + 6% CNT, Mg + 8% CNT | 70.3 HV | 265.5 MPa | - | - | [1] |
| 21. | Magnesium powder 99.9% pure, Carbon nanotubes | Mg + 0.8% CNT | - | 238 MPa | - | - | [32] |

It is observed from Table 8 that multi-walled short CNT-reinforced AZ91D composite has the highest tensile strength of 388 MPa [116–121]. Whereas, Carbon nanotubes and Aluminium powder reinforced Mg composite and Copper powder and Graphene nanoplatelets reinforced Mg composite has the highest compressive strength of 421 MPa and 420 MPa, respectively [106–110]. Although, the highest microhardness is obtained at 92 HV in the case of the $B_4C$-reinforced Mg composite [82].

Fabrication of Mg matrix composites within design constraints remains a significant problem for academics and manufacturers [122–125]. With this goal in mind, the current study examined the performance of previously synthesised Mg matrix composites.

## 6. Conclusions

In order to enhance the engineering use of Mg MMCs, a number of challenges must be overcome, including manufacturing methods, the influence of reinforcement on mechanical and microstructure characteristics, and applications. The key findings drawn from previous research are summarised as follows:

- When compared to alternative production processes such as stir casting, friction stir processing, and so on, a thorough literature review revealed that the powder metallurgy approach is the most straightforward way to synthesize metal matrix composites

with hard and soft reinforcements. When composites are produced via the powder metallurgy technique, proper bonding between the matrix material and reinforcements occurs. The study found that composites made with powder metallurgy had better mechanical and tribological characteristics than those made with other methods.

- The addition of carbon nanotubes to the magnesium and magnesium alloy matrix enhanced the composites' wettability and bonding strength. $Al_2O_3$-reinforced magnesium matrix composites outperform CNT-reinforced magnesium matrix composites in terms of wear resistance. When compared to $Al_2O_3$-reinforced magnesium MMCs, SiC-particle-reinforced magnesium MMCs exhibit better wear and creep resistance. Boron Carbide ($B_4C$) has been shown to improve the interfacial bonding strength and flexural strength of hybrid composites when added to the magnesium matrix. The tensile strength of a magnesium matrix composite is enhanced by adding fibres, but the ductility is decreased.
- Magnesium MMCs' creep behaviour is governed by the matrix's creep, which is primarily responsible for regulating dislocation viscous slip and, to a lesser extent, grain boundary slippage.
- Scholars and scientists working in the domain of magnesium metal matrix composites using the powder metallurgy technique will benefit from this article.

**Author Contributions:** Conceptualization, G.S.A., K.K.S. and C.P.; methodology, K.A.M.; writing—original draft preparation, G.S.A. and K.K.S.; writing—review and editing, C.P. and S.D. All authors have read and agreed to the published version of the manuscript.

**Funding:** The research is partially funded by the Ministry of Science and Higher Education of the Russian Federation under the strategic academic leadership program 'Priority 2030' (Agreement 075-15-2021-1333 dated 30 September 2021).

**Institutional Review Board Statement:** Not applicable.

**Informed Consent Statement:** Not applicable.

**Data Availability Statement:** Not applicable.

**Conflicts of Interest:** The authors declare no conflict of interest.

## References

1. Li, H.; Dai, X.; Zhao, L.; Li, B.; Wang, H.; Liang, C.; Fan, J. Microstructure and properties of carbon nanotubes-reinforced magnesium matrix composites fabricated via novel in situ synthesis process. *J. Alloys Compd.* **2019**, *785*, 146–155. [CrossRef]
2. Han, G.; Wang, Z.; Liu, K.; Li, S.; Du, X.; Du, W. Synthesis of CNT-reinforced AZ31 magnesium alloy composites with uniformly distributed CNTs. *Mater. Sci. Eng. A* **2015**, *628*, 350–357. [CrossRef]
3. Ali, Y.; Qiu, D.; Jiang, B.; Pan, F.; Zhang, M.-X. Current research progress in grain refinement of cast magnesium alloys: A review article. *J. Alloys Compd.* **2014**, *619*, 639–651. [CrossRef]
4. Wang, L.; Mostaed, E.; Cao, X.; Huang, G.; Fabrizi, A.; Bonollo, F.; Chi, C.; Vedani, M. Effects of texture and grain size on mechanical properties of AZ80 magnesium alloys at lower temperatures. *Mater. Des.* **2016**, *89*, 1–8. [CrossRef]
5. Zhang, L.; Wang, Q.; Liao, W.; Guo, W.; Li, W.; Jiang, H.; Ding, W. Microstructure and mechanical properties of the carbon nanotubes reinforced AZ91D magnesium matrix composites processed by cyclic extrusion and compression. *Mater. Sci. Eng. A* **2017**, *689*, 427–434. [CrossRef]
6. Rashad, M.; Pan, F.; Asif, M.; Ullah, A. Improved mechanical properties of magnesium–graphene composites with copper–graphene hybrids. *Mater. Sci. Technol.* **2014**, *31*, 1452–1461. [CrossRef]
7. Garcés, G.; Rodríguez, M.; Pérez, P.; Adeva, P. Effect of volume fraction and particle size on the microstructure and plastic deformation of Mg–$Y_2O_3$ composites. *Mater. Sci. Eng. A* **2006**, *419*, 357–364. [CrossRef]
8. Nguyen, Q.; Gupta, M. Increasing significantly the failure strain and work of fracture of solidification processed AZ31B using nano-$Al_2O_3$ particulates. *J. Alloys Compd.* **2008**, *459*, 244–250. [CrossRef]
9. Huard, G.; Angers, R.; Krishnadev, M.R.; Tremblay, R.; Dube, D. SiCp/Mg Composites Made by Low-Energy Mechanical Processing. *Can. Metall. Q.* **2013**, *38*, 193–200. [CrossRef]
10. Wen, C.E.; Yamada, Y.; Shimojima, K.; Chino, Y.; Hosokawa, H.; Mabuchi, M. Compressibility of porous magnesium foam: Dependency on porosity and pore size. *Mater. Lett.* **2004**, *58*, 357–360. [CrossRef]
11. Zhou, S.-S.; Deng, K.-K.; Li, J.-C.; Shang, S.-J.; Liang, W.; Fan, J.-F. Effects of volume ratio on the microstructure and mechanical properties of particle reinforced magnesium matrix composite. *Mater. Des.* **2014**, *63*, 672–677. [CrossRef]

12. Wong, E.W.; Sheehan, P.E.; Lieber, C.M. Nanobeam Mechanics: Elasticity, Strength, and Toughness of Nanorods and Nanotubes. *Science* **1997**, *277*, 1971–1975. [CrossRef]
13. Yu, M.-F.; Lourie, O.; Dyer, M.J.; Moloni, K.; Kelly, T.F.; Ruoff, R.S. Strength and Breaking Mechanism of Multiwalled Carbon Nanotubes Under Tensile Load. *Science* **2000**, *287*, 637–640. [CrossRef] [PubMed]
14. Nai, M.H.; Wei, J.; Gupta, M. Interface tailoring to enhance mechanical properties of carbon nanotube reinforced magnesium composites. *Mater. Des.* **2014**, *60*, 490–495. [CrossRef]
15. Habibi, M.K.; Paramsothy, M.; Hamouda, A.M.S.; Gupta, M. Enhanced compressive response of hybrid Mg–CNT nano-composites. *J. Mater. Sci.* **2011**, *46*, 4588–4597. [CrossRef]
16. Li, C.; Wang, X.; Liu, W.; Shi, H.; Ding, C.; Hu, X.; Zheng, M.; Wu, K. Effect of solidification on microstructures and mechanical properties of carbon nanotubes reinforced magnesium matrix composite. *Mater. Des.* **2014**, *58*, 204–208. [CrossRef]
17. Zou, N.; Li, Q. Compressive mechanical property of porous magnesium composites reinforced by carbon nanotubes. *J. Mater. Sci.* **2016**, *51*, 5232–5239. [CrossRef]
18. Carreño-Morelli, E.; Yang, J.; Couteau, E.; Hernadi, K.; Seo, J.W.; Bonjour, C.; Schaller, R. Carbon nanotube/magnesium composites. *Phys. Status Solidi (A)* **2004**, *201*, R53–R55. [CrossRef]
19. Sabetghadam-Isfahani, A.; Abbasi, M.; Sharifi, S.; Fattahi, M.; Amirkhanlou, S. Microstructure and mechanical properties of carbon nanotubes/AZ31 magnesium composite gas tungsten arc welding filler rods fabricated by powder metallurgy. *Diam. Relat. Mater.* **2016**, *69*, 160–165. [CrossRef]
20. Li, C.; Wang, X.; Liu, W.; Wu, K.; Shi, H.; Ding, C.; Hu, X.; Zheng, M. Microstructure and strengthening mechanism of carbon nanotubes reinforced magnesium matrix composite. *Mater. Sci. Eng. A* **2014**, *597*, 264–269. [CrossRef]
21. Yuan, X.; Zhu, H.; Ji, H.; Zhang, Y. Effect of CNT contents on the microstructure and properties of CNT/TiMg composites. *Materials.* **2019**, *12*, 1620. [CrossRef] [PubMed]
22. Abazari, S.; Shamsipur, A.; Bakhsheshi-Rad, H.R.; Ismail, A.F.; Sharif, S.; Razzaghi, M.; Ramakrishna, S.; Berto, F. Carbon nanotubes (CNTs)-reinforced magnesium-based matrix composites: A comprehensive review. *Materials* **2020**, *13*, 4421. [CrossRef] [PubMed]
23. Prakash, C.; Singh, S.; Basak, A.; Krolczyk, G.; Pramanik, A.; Lamberti, L.; Pruncu, C.I. Processing of $Ti_{50}Nb_{50-x}HA_x$ composites by rapid microwave sintering technique for biomedical applications. *J. Mater. Res. Technol.* **2019**, *9*, 242–252. [CrossRef]
24. Prakash, C.; Singh, S.; Pramanik, A.; Basak, A.; Królczyk, G.; Bogdan-Chudy, M.; Wu, Y.L.; Zheng, H.Y. Experi-mental investigation into nano-finishing of β-TNTZ alloy using magnetorheological fluid magnetic abrasive finishing process for orthopedic applications. *J. Mater. Res. Technol.* **2021**, *11*, 600–617. [CrossRef]
25. Singh, S.; Prakash, C. Effect of cryogenic treatment on the microstructure, mechanical properties and finishability of β-TNTZ alloy for orthopedic applications. *Mater. Lett.* **2020**, *278*, 128461. [CrossRef]
26. Singh, H.; Prakash, C.; Singh, S. Plasma spray deposition of HA-$TiO_2$ on β-phase Ti-$_{35}$Nb-$_7$Ta-$_5$Zr alloy for hip stem: Characterization of bio-mechanical properties, wettability, and wear resistance. *J. Bionic Eng.* **2020**, *17*, 1029–1044. [CrossRef]
27. Prakash, C.; Singh, S.; Ramakrishna, S.; Królczyk, G.; Le, C.H. Microwave sintering of porous Ti–Nb-HA compo-site with high strength and enhanced bioactivity for implant applications. *J. Alloys Compd.* **2020**, *824*, 153774. [CrossRef]
28. Pradhan, S.; Singh, S.; Prakash, C.; Królczyk, G.; Pramanik, A.; Pruncu, C.I. Investigation of machining characteris-tics of hard-to-machine Ti-6Al-4V-ELI alloy for biomedical applications. *J. Mater. Res. Technol.* **2019**, *8*, 4849–4862. [CrossRef]
29. Prakash, C.; Singh, S.; Ramakrishna, S. Characterization of indigenously coated biodegradable magnesium alloy primed through novel additive manufacturing assisted investment casting. *Mater. Lett.* **2020**, *275*, 128137. [CrossRef]
30. Singh, G.; Singh, S.; Prakash, C.; Ramakrishna, S. On investigating the soda-lime shot blasting of AZ31 alloy: Ef-fects on surface roughness, material removal rate, corrosion resistance, and bioactivity. *J. Magnes. Alloy.* **2021**, *9*, 1272–1284. [CrossRef]
31. Prakash, C.; Singh, S.; Farina, I.; Fraternali, F.; Feo, L. Physical-mechanical characterization of biodegradable Mg-3Si-HA composites. *PSU Res. Rev.* **2018**, *2*, 152–174. [CrossRef]
32. Mohan, N.; Senthil, P.; Vinodh, S.; Jayanth, N. A review on composite materials and process parameters optimisation for the fused deposition modelling process. *Virtual Phys. Prototyp.* **2017**, *12*, 47–59. [CrossRef]
33. Xiao, J.; Shu, D.W.; Wang, X. Effect of strain rate and temperature on the mechanical behavior of magnesium nanocomposites. *Int. J. Mech. Sci.* **2014**, *89*, 381–390. [CrossRef]
34. Zengin, H.; Turen, Y. Effect of La content and extrusion temperature on microstructure, texture and mechanical properties of Mg-Zn-Zr magnesium alloy. *Mater. Chem. Phys.* **2018**, *214*, 421–430. [CrossRef]
35. Shen, J.; Yin, W.; Kondoh, K.; Jones, T.L.; Kecskes, L.J.; Yarmolenko, S.N.; Wei, Q. Mechanical behavior of a lantha-num-doped magnesium alloy at different strain rates. *Mater. Sci. Eng. A* **2015**, *626*, 108–121. [CrossRef]
36. Malik, A.; Chaudry, U.M.; Yan, T.; Long, J.; Li, C.; Wang, Y. Achieving higher dynamic me-chanical response by adjusting texture through twinning in a ZK61 Mg alloy. *J. Alloys Compd.* **2022**, *902*, 163755. [CrossRef]
37. Rashad, M.; Pan, F.; Asif, M.; She, J.; Ullah, A. Improved mechanical proprieties of "magnesium based composites" with titanium–aluminum hybrids. *J. Magnes. Alloy.* **2015**, *3*, 1–9. [CrossRef]
38. Aatthisugan, I.; Rose, A.R.; Jebadurai, D.S. Mechanical and wear behaviour of AZ91D magnesium matrix hybrid composite reinforced with boron carbide and graphite. *J. Magnes. Alloy.* **2017**, *5*, 20–25. [CrossRef]
39. Xiang, S.; Wang, X.; Gupta, M.; Wu, K.; Hu, X.; Zheng, M. Graphene nanoplatelets induced heterogeneous bimodal structural magnesium matrix composites with enhanced mechanical properties. *Sci. Rep.* **2016**, *6*, 38824. [CrossRef]

40. Malik, A.; Wang, Y.; Huanwu, C.; Nazeer, F.; Ahmed, B.; Khan, M.A.; Mingjun, W. Constitutive analysis, twinning, recrystallization, and crack in fine-grained ZK61 Mg alloy during high strain rate com-pression over a wide range of temperatures. *Mater. Sci. Eng. A* **2020**, *771*, 138649. [CrossRef]
41. Arokiasamy, S.; Ronald, B.A. Experimental investigations on the enhancement of mechanical properties of magnesium-based hybrid metal matrix composites through friction stir processing. *Int. J. Adv. Manuf. Technol.* **2017**, *93*, 493–503. [CrossRef]
42. Prakash, C.; Singh, S.; Gupta, M.K.; Mia, M.; Królczyk, G.; Khanna, N. Synthesis, characterization, corrosion re-sistance and in-vitro bioactivity behavior of biodegradable Mg–Zn–Mn–(Si–HA) composite for orthopaedic applica-tions. *Materials* **2018**, *11*, 1602. [CrossRef] [PubMed]
43. Shang, Y.; Pistidda, C.; Gizer, G.; Klassen, T.; Dornheim, M. Mg-based materials for hydrogen storage. *J. Magnes. Alloy.* **2021**, *9*, 1837–1860. [CrossRef]
44. Wu, L.; Wu, R.; Hou, L.; Zhang, J.; Sun, J.; Zhang, M. Microstructure and Mechanical Properties of CNT-Reinforced AZ31 Matrix Composites Prepared Using Hot-Press Sintering. *J. Mater. Eng. Perform.* **2017**, *26*, 5495–5500. [CrossRef]
45. Mishra, M.; Prakash, C.; Shabadi, R.; Singh, S. Mechanical and microstructural characterization of magnesi-um/multi-walled carbon nanotubes composites fabricated via friction stir processing. In *Advances in Materials Science and Engineering*; Springer: Singapore, 2020; pp. 137–147.
46. Srichok, T.; Pitakaso, R.; Sethanan, K.; Sirirak, W.; Kwangmuang, P. Combined response surface method and modified differential evolution for parameter optimization of friction stir welding. *Processes* **2020**, *8*, 1080. [CrossRef]
47. Khodabakhshi, F.; Yazdabadi, H.G.; Kokabi, A.; Simchi, A. Friction stir welding of a P/M Al–$Al_2O_3$ nanocomposite: Microstructure and mechanical properties. *Mater. Sci. Eng. A* **2013**, *585*, 222–232. [CrossRef]
48. Raheja, G.S.; Singh, S.; Prakash, C. Processing and characterization of Al5086-Gr-SiC hybrid surface composite using friction stir technique. *Mater. Today Proc.* **2020**, *28*, 1350–1354. [CrossRef]
49. Singh, S.; Singh, G.; Prakash, C.; Kumar, R. On the mechanical characteristics of friction stir welded dissimilar polymers: Statistical analysis of the processing parameters and morphological investigations of the weld joint. *J. Braz. Soc. Mech. Sci. Eng.* **2020**, *42*, 1–12. [CrossRef]
50. Mishra, R.; Mahoney, M.; McFadden, S.; Mara, N.; Mukherjee, A. High strain rate superplasticity in a friction stir processed 7075 Al alloy. *Scr. Mater.* **1999**, *42*, 163–168. [CrossRef]
51. Dinaharan, I.; Zhang, S.; Chen, G.; Shi, Q. Development of titanium particulate reinforced AZ31 magnesium matrix composites via friction stir processing. *J. Alloys Compd.* **2019**, *820*, 153071. [CrossRef]
52. Alam, N.; Iqbal, M.; Prakash, C.; Singh, S.; Basak, A. Influence of the microstructural and mechanical properties of reinforced graphene in magnesium matrix fabricated by friction stir processing. In *Advances in Materials Science and Engineering*; Springer: Singapore, 2020; pp. 235–247.
53. Sánchez de la Muela, A.M.; Duarte, J.; Santos Baptista, J.; García Cambronero, L.E.; Ruiz-Román, J.M.; Elorza, F.J. Stir Casting Routes for Processing Metal Matrix Syntactic Foams: A Scoping Review. *Processes* **2022**, *10*, 478. [CrossRef]
54. Lu, D.; Jiang, Y.; Zhou, R. Wear performance of nano-$Al_2O_3$ particles and CNTs reinforced magnesium matrix composites by friction stir processing. *Wear* **2013**, *305*, 286–290. [CrossRef]
55. Ahmadkhaniha, D.; Sohi, M.H.; Salehi, A.; Tahavvori, R. Formations of AZ91/$Al_2O_3$ nano-composite layer by friction stir processing. *J. Magnes. Alloy.* **2016**, *4*, 314–318. [CrossRef]
56. Dinaharan, I.; Zhang, S.; Chen, G.; Shi, Q. Titanium particulate reinforced AZ31 magnesium matrix composites with improved ductility prepared using friction stir processing. *Mater. Sci. Eng. A* **2019**, *772*, 138793. [CrossRef]
57. Sajjadi, S.; Ezatpour, H.; Beygi, H. Microstructure and mechanical properties of Al–$Al_2O_3$ micro and nano composites fabricated by stir casting. *Mater. Sci. Eng. A* **2011**, *528*, 8765–8771. [CrossRef]
58. Ezatpour, H.; Torabi-Parizi, M.; Sajjadi, S.A. Microstructure and mechanical properties of extruded Al/$Al_2O_3$ composites fabricated by stir-casting process. *Trans. Nonferrous Met. Soc. China* **2013**, *23*, 1262–1268. [CrossRef]
59. Sajjadi, S.; Ezatpour, H.; Parizi, M.T. Comparison of microstructure and mechanical properties of A356 aluminum alloy/$Al_2O_3$ composites fabricated by stir and compo-casting processes. *Mater. Des.* **2012**, *34*, 106–111. [CrossRef]
60. Ezatpour, H.R.; Sajjadi, S.A.; Sabzevar, M.H.; Huang, Y. Investigation of microstructure and mechanical properties of Al6061-nanocomposite fabricated by stir casting. *Mater. Des.* **2014**, *55*, 921–928. [CrossRef]
61. Rashad, M.; Pan, F.; Liu, Y.; Chen, X.; Lin, H.; Pan, R.; Asif, M.; She, J. High temperature formability of graphene nanoplatelets-AZ31 composites fabricated by stir-casting method. *J. Magnes. Alloy.* **2016**, *4*, 270–277. [CrossRef]
62. Ramanathan, A.; Krishnan, P.K.; Muraliraja, R. A review on the production of metal matrix composites through stir casting—Furnace design, properties, challenges, and research opportunities. *J. Manuf. Process.* **2019**, *42*, 213–245. [CrossRef]
63. Yu, W.; Wang, X.; Zhao, H.; Ding, C.; Huang, Z.; Zhai, H.; Guo, Z.; Xiong, S. Microstructure, mechanical properties and fracture mechanism of $Ti_2AlC$ reinforced AZ91D composites fabricated by stir casting. *J. Alloys Compd.* **2017**, *702*, 199–208. [CrossRef]
64. Chelliah, N.M.; Singh, H.; Surappa, M. Correlation between microstructure and wear behavior of AZX915 Mg-alloy reinforced with 12 wt.% TiC particles by stir-casting process. *J. Magnes. Alloy.* **2016**, *4*, 306–313. [CrossRef]
65. Khandelwal, A.; Mani, K.; Srivastava, N.; Gupta, R.; Chaudhari, G. Mechanical behavior of AZ31/$Al_2O_3$ magnesium alloy nanocomposites prepared using ultrasound assisted stir casting. *Compos. Part B Eng.* **2017**, *123*, 64–73. [CrossRef]

66. Wang, X.; Wang, N.; Wang, L.; Hu, X.; Wu, K.; Wang, Y.; Huang, Y. Processing, microstructure and mechanical properties of micro-SiC particles reinforced magnesium matrix composites fabricated by stir casting assisted by ultrasonic treatment processing. *Mater. Des.* **2014**, *57*, 638–645. [CrossRef]
67. Sameer, K.D.; Suman, K.N.S.; Tara, S.C.; Ravindra, K.; Palash, P.; Venkata Siva, S.B. Microstructure, mechanical response and fractography of AZ91E/$Al_2O_3$ (p) nano composite fabricated by semi solid stir casting method. *J. Magnes. Alloy.* **2017**, *5*, 48–55. [CrossRef]
68. Abbas, A.; Huang, S.J.; Ballóková, B.; Sülleiová, K. Tribological effects of carbon nanotubes on magnesium alloy AZ31 and analyzing aging effects on CNTs/AZ31 composites fabricated by stir casting process. *Tribol. Int.* **2019**, *142*, 105982. [CrossRef]
69. Prakash, C.; Singh, S.; Pabla, B.S.; Sidhu, S.S.; Uddin, M. Bio-inspired low elastic biodegradable Mg-Zn-Mn-Si-HA alloy fabricated by spark plasma sintering. *Mater. Manuf. Process.* **2018**, *34*, 357–368. [CrossRef]
70. Xue, Z.; Han, X.; Zhou, Z.; Wang, Y.; Li, X.; Wu, J. Effects of Microstructure and Texture Evolution on Strength Improvement of an Extruded Mg-10Gd-2Y-0.5 Zn-0.3 Zr Alloy. *Metals* **2018**, *8*, 1087. [CrossRef]
71. Youh, M.-J.; Huang, Y.-R.; Peng, C.-H.; Lin, M.-H.; Chen, T.-Y.; Chen, C.-Y.; Liu, Y.-M.; Pu, N.-W.; Liu, B.-Y.; Chou, C.-H.; et al. Using Graphene-Based Composite Materials to Boost Anti-Corrosion and Infrared-Stealth Performance of Epoxy Coatings. *Nanomaterials* **2021**, *11*, 1603. [CrossRef]
72. Singh, B.P.; Singh, R.; Mehta, J.S.; Prakash, C. August. Fabrication of biodegradable low elastic porous Mg-Zn-Mn-HA alloy by spark plasma sintering for orthopaedic applications. In *Materials Science and Engineering*; IOP Conference Series; IOP Publishing: Bristol, UK, 2017; Volume 225, p. 012050.
73. Prakash, C.; Singh, S.; Abdul-Rani, A.M.; Uddin, M.S.; Pabla, B.S.; Puri, S. Spark plasma sintering of Mg-Zn-Mn-Si-HA alloy for bone fixation devices: Fabrication of biodegradable low elastic porous Mg-Zn-Mn-Si-HA alloy. In *Handbook of Research on Green Engineering Techniques for Modern Manufacturing*; IGI Global: Hershey, PA, USA, 2019; pp. 282–295.
74. Hidalgo, A.A.; Frykholm, R.; Ebel, T.; Pyczak, F. Powder Metallurgy Strategies to Improve Properties and Processing of Titanium Alloys: A Review. *Adv. Eng. Mater.* **2017**, *19*, 1600743. [CrossRef]
75. Dinaharan, I.; Akinlabi, E.T. Low cost metal matrix composites based on aluminum, magnesium and copper reinforced with fly ash prepared using friction stir processing. *Compos. Commun.* **2018**, *9*, 22–26. [CrossRef]
76. Li, C.P.; Wang, Z.G.; Zha, M.; Wang, C.; Yu, H.C.; Wang, H.Y.; Jiang, Q.C. Effect of pre-oxidation treatment of Nano-SiC particulates on microstructure and mechanical properties of SiC/Mg-8Al-1Sn composites fabricated by powder metallurgy combined with hot extrusion. *Materials* **2016**, *9*, 964. [CrossRef] [PubMed]
77. Shimizu, Y.; Miki, S.; Soga, T.; Itoh, I.; Todoroki, H.; Hosono, T.; Sakaki, K.; Hayashi, T.; Kim, Y.; Endo, M.; et al. Multi-walled carbon nanotube-reinforced magnesium alloy composites. *Scr. Mater.* **2008**, *58*, 267–270. [CrossRef]
78. Du, X.M.; Zhen, K.F.; Liu, F.G. Graphene reinforced magnesium matrix composites by hot pressed sintering. *Dig. J. Nanomater. Bios* **2018**, *13*, 827–833.
79. Munir, K.; Wen, C.; Li, Y. Graphene nanoplatelets-reinforced magnesium metal matrix nanocomposites with superior mechanical and corrosion performance for biomedical applications. *J. Magnes. Alloy.* **2020**, *8*, 269–290. [CrossRef]
80. Purohit, R.; Dewang, Y.; Rana, R.S.; Koli, D.; Dwivedi, S. Fabrication of magnesium matrix composites using powder metallurgy process and testing of properties. *Mater. Today Proc.* **2018**, *5*, 6009–6017. [CrossRef]
81. Chiu, C.; Huang, H.M. Microstructure and properties of Mg-Zn-Y alloy powder compacted by equal channel angular pressing. *Materials* **2018**, *11*, 1678. [CrossRef]
82. Nickel, D.; Dietrich, D.; Mehner, T.; Frint, P.; Spieler, D.; Lampke, T. Effect of strain localization on pitting corrosion of an AlMgSi0.5 alloy. *Metals* **2015**, *5*, 172–191. [CrossRef]
83. Satish, J.; Satish, K. Preparation of magnesium metal matrix composites by powder metallurgy process. *IOP Conf. Ser. Mater. Sci. Eng.* **2018**, *310*, 012130. [CrossRef]
84. Dey, A.; Pandey, K.M. Magnesium metal matrix composites—A review. *Rev.Adv. Mater. Sci.* **2015**, *42*, 58–67.
85. Ye, H.Z.; Liu, X.Y. Review of recent studies in magnesium matrix composites. *J. Mater. Sci.* **2004**, *39*, 6153–6171. [CrossRef]
86. Iijima, S. Helical microtubules of graphitic carbon. *Nature* **1991**, *354*, 56–58. [CrossRef]
87. Li, Q.; Tian, B. Compression behavior of magnesium/carbon nanotube composites. *J. Mater. Res.* **2013**, *28*, 1877–1884. [CrossRef]
88. Kondoh, K.; Fukuda, H.; Umeda, J.; Imai, H.; Fugetsu, B.; Endo, M. Microstructural and mechanical analysis of carbon nanotube reinforced magnesium alloy powder composites. *Mater. Sci. Eng. A* **2010**, *527*, 4103–4108. [CrossRef]
89. Umeda, J.; Kondoh, K.; Imai, H. Friction and wear behavior of sintered magnesium composite reinforced with CNT-$Mg_2Si$/MgO. *Mater. Sci. Eng. A* **2009**, *504*, 157–162. [CrossRef]
90. Choi, W.; Lahiri, I.; Seelaboyina, R.; Kang, Y.S. Synthesis of Graphene and Its Applications: A Review. *Crit. Rev. Solid State Mater. Sci.* **2010**, *35*, 52–71. [CrossRef]
91. Kumar, H.P.; Xavior, M.A. Graphene Reinforced Metal Matrix Composite (GRMMC): A Review. *Procedia Eng.* **2014**, *97*, 1033–1040. [CrossRef]
92. Tabandeh-Khorshid, M.; Kumar, A.; Omrani, E.; Kim, C.; Rohatgi, P. Synthesis, characterization, and properties of graphene reinforced metal-matrix nanocomposites. *Compos. Part B Eng.* **2019**, *183*, 107664. [CrossRef]
93. Naseer, A.; Ahmad, F.; Aslam, M.; Guan, B.H.; Harun, W.S.W.; Muhamad, N.; Raza, M.R.; German, R.M. A review of processing techniques for graphene-reinforced metal matrix composites. *Mater. Manuf. Process.* **2019**, *34*, 957–985. [CrossRef]

94. Raja, K.S.; Kumar, U.M.; Mathivanan, S.; Ganesan, S.; ArunKumar, T.; Hemanandh, J.; Kumar, J.S. Mechanical and microstructural properties of graphene reinforced magnesium composite. *Mater. Today Proc.* **2020**, *44*, 3571–3574. [CrossRef]
95. Rashad, M.; Pan, F.; Tang, A.; Asif, M. Effect of graphene nanoplatelets addition on mechanical properties of pure aluminum using a semi-powder method. *Prog. Nat. Sci. Mater. Int.* **2014**, *24*, 101–108. [CrossRef]
96. Tabandeh-Khorshid, M.; Omrani, E.; Menezes, P.L.; Rohatgi, P.K. Tribological performance of self-lubricating aluminum matrix nanocomposites: Role of graphene nanoplatelets. *Eng. Sci. Technol. Int. J.* **2016**, *19*, 463–469. [CrossRef]
97. Sharma, S.K.; Saxena, K.K. An outlook on the influence on mechanical properties of AZ31 reinforced with graphene nanoparticles using powder metallurgy technique for biomedical application. *Mater. Today Proc.* **2022**, *56*, 2278–2287. [CrossRef]
98. Rashad, M.; Pan, F.; Asif, M.; Tang, A. Powder metallurgy of Mg–1%Al–1%Sn alloy reinforced with low content of graphene nanoplatelets (GNPs). *J. Ind. Eng. Chem.* **2014**, *20*, 4250–4255. [CrossRef]
99. Lim, C.; Leo, D.; Ang, J.; Gupta, M. Wear of magnesium composites reinforced with nano-sized alumina particulates. *Wear* **2005**, *259*, 620–625. [CrossRef]
100. Rashad, M.; Pan, F.; Guo, W.; Lin, H.; Asif, M.; Irfan, M. Effect of alumina and silicon carbide hybrid reinforcements on tensile, compressive and microhardness behavior of Mg–3Al–1Zn alloy. *Mater. Charact.* **2015**, *106*, 382–389. [CrossRef]
101. Dixit, S.; Sharma, K. An Empirical Study of Major Factors Affecting Productivity of Construction Projects. In *Lecture Notes in Civil Engineering*; Springer: Singapore, 2020; Volume 61. [CrossRef]
102. Dixit, S.; Singh, S.; Singh, S.; Varghese, R.G.; Pandey, A.K.; Varshney, D. Role of Solar energy and issues in its implementation in the Indian context. In Proceedings of the ICDAMS 2018, Saveetha School of Engineering, Chennai, Tamil Nadu, India, 6–7 April 2018; Volume 172, p. 06001. [CrossRef]
103. Dixit, S. Analysing the Impact of Productivity in Indian Transport Infra Projects. In IOP Conference Series: Materials Science and Engineering, Proceedings of the Creative Construction Conference (CCC 2021), Budapest, Hungary, 28–30 June 2021; Volume 1218, p. 12059.
104. Dixit, S.; Arora, R.; Kumar, K.; Bansal, S.; Vatin, N.; Araszkiewicz, K.; Epifantsev, K. Replacing E-waste with coarse aggregate in architectural engineering and construction industry. *Mater. Today Proc.* **2021**, *56*, 2353–2358. [CrossRef]
105. Dixit, S.; Mandal, S.N.; Thanikal, J.V.; Saurabh, K. Evolution of studies in construction productivity: A systematic literature review (2006–2017). *Ain Shams Eng. J.* **2019**, *10*, 555–564. [CrossRef]
106. Dixit, S.; Sharma, K.; Ingh, S. Identifying and Analysing Key Factors Associated with Risks in Construction Projects. In *Emerging Trends in Civil Engineering*; Babu, K.G., Rao, H.S., Amarnath, Y., Eds.; Springer: Singapore, 2020; pp. 25–32.
107. Dixit, S.; Stefańska, A. Digitisation of contemporary fabrication processes in the AEC sector. *Mater. Today Proc.* **2021**, *56*, 1882–1885. [CrossRef]
108. Dixit, S.; Stefańska, A.; Singh, P. Manufacturing technology in terms of digital fabrication of contemporary biomimetic structures. *Int. J. Constr. Manag.* **2021**, 1–9. [CrossRef]
109. Kumar, K.; Arora, R.; Khan, S.; Dixit, S. Characterization of fly ash for potential utilization in green concrete. *Mater. Today Proc.* **2021**, *56*, 1886–1890. [CrossRef]
110. Rai, R.K.; Gosain, A.K.; Singh, P.; Dixit, S. Farm Advisory Services for Farmers Using SWAT and APEX Model. In *International Conference Sustainable Energy Systems: Innovative Perspectives*; Springer: Cham, Switzerland, 2020; pp. 444–458.
111. Shah, M.N.; Dixit, S.; Kumar, R.; Jain, R.; Anand, K. Causes of delays in slum reconstruction projects in India. *Int. J. Constr. Manag.* **2019**, *21*, 452–467. [CrossRef]
112. Singh, P.; Dixit, S.; Sammanit, D.; Krishnan, P. The Automated Farmlands of Tomorrow: An IoT Integration with Farmlands. IOP Conference Series: Materials Science and Engineering, Creative Construction Conference (CCC 2021), Budapest, Hungary, 28–30 June 2021; 1218, p. 12048.
113. Singh, S.; Dixit, S.; Sahai, S.; Sao, A.; Kalonia, Y.; Kumar, R.S. Key Benefits of Adopting Lean Manufacturing Principles in Indian Construction Industry. *MATEC Web Conf.* **2018**, *172*, 05002. [CrossRef]
114. Gu, J.; Zhang, X.; Qiu, Y.; Gu, M. Damping behaviors of magnesium matrix composites reinforced with Cu-coated and uncoated SiC particulates. *Compos. Sci. Technol.* **2005**, *65*, 1736–1742. [CrossRef]
115. Lim, C.; Lim, S.; Gupta, M. Wear behaviour of SiCp-reinforced magnesium matrix composites. *Wear* **2003**, *255*, 629–637. [CrossRef]
116. Saravanan, R.; Surappa, M. Fabrication and characterisation of pure magnesium-30 vol.% SiCP particle composite. *Mater. Sci. Eng. A* **2000**, *276*, 108–116. [CrossRef]
117. Jiang, Q.; Wang, H.; Ma, B.; Wang, Y.; Zhao, F. Fabrication of $B_4C$ particulate reinforced magnesium matrix composite by powder metallurgy. *J. Alloys Compd.* **2005**, *386*, 177–181. [CrossRef]
118. Badini, C.; Marino, F.; Montorsi, M.; Guo, X. Precipitation phenomena in $B_4C$-reinforced magnesium-based composite. *Mater. Sci. Eng. A* **1992**, *157*, 53–61. [CrossRef]
119. Gopal Krishna, U.B.; Sreenivas Rao, K.V.; Vasudeva, B. Effect of percentage reinforcement of $B_4C$ on the tensile property of aluminium matrix composites. *Int. J. Mech. Eng. Robot. Res.* **2012**, *1*, 290–295.
120. Rashad, M.; Pan, F.; Tang, A.; Asif, M.; She, J.; Gou, J.; Mao, J.; Hu, H. Development of magnesium-graphene nanoplatelets composite. *J. Compos. Mater.* **2014**, *49*, 285–293. [CrossRef]
121. Rashad, M.; Pan, F.; Tang, A.; Asif, M.; Hussain, S.; Gou, J.; Mao, J. Improved strength and ductility of magnesium with addition of aluminum and graphene nanoplatelets (Al+GNPs) using semi powder metallurgy method. *J. Ind. Eng. Chem.* **2015**, *23*, 243–250. [CrossRef]

122. Tripathi, D.R.; Vachhani, K.H.; Bandhu, D.; Kumari, S.; Kumar, V.R.; Abhishek, K. Experimental investigation and op-timization of abrasive waterjet machining parameters for GFRP composites using metaphor-less algorithms. *Mater. Manuf. Processes* **2021**, *36*, 803–813. [CrossRef]
123. Bandhu, D.; Vora, J.J.; Das, S.; Thakur, A.; Kumari, S.; Abhishek, K.; Sastry, M.N. Experimental study on application of gas metal arc welding based regulated metal deposition technique for low alloy steel. *Mater. Manuf. Processes* **2022**, *37*, 1–19. [CrossRef]
124. Sonia, P.; Kumari, S. Performance Evaluation Of Multi-Fibre (Hybrid) Polymer Composite. *IOP Conf. Series Mater. Sci. Eng.* **2021**, *1116*, 012027. [CrossRef]
125. Kumari, S.; Nakum, B.; Bandhu, D.; Abhishek, K. Multi-Attribute Group Decision Making (MAGDM) Using Fuzzy Lin-guistic Modeling Integrated With the VIKOR Method for Car Purchasing Model. *Int. J. Decis. Support Syst. Technol.* **2022**, *14*, 1–20. [CrossRef]